Effects of superhydrophobic SiO_2 nano-particles on the performance of PVDF flat sheet membranes for Membrane distillation

Johnson E. Efome

A thesis submitted to the

Faculty of Graduate and Postdoctoral Studies in partial fulfillment of the requirements for the

Masters of Applied Science in Chemical Engineering

University of Ottawa

Abstract

Poly(vinylidene) fluoride (PVDF) nano-composite membranes were prepared. The dope solution contained varied concentrations of superhydrophobic SiO_2 nano-particles. The fabricated flat sheet membranes were characterized extensively by SEM, FTIR, water contact angle, LEP_w, surface roughness, pore size diameter and pore size distribution. The effect of the nano-particles on the membrane performance was then analysed. The nano-composite membranes showed increased surface pore diameter, elevated water contact angle measurements with lower LEP_w when compared to the neat membrane. The 7 wt. % nano-composite membrane showed the greatest flux in a VMD process with 2.9 $kg/m^2.h$ flux achieved accounting to a 4 fold increase when compared to the neat membrane. Desalination test were carried out using a 35 g/L synthetic salt water and rejection >99.98% was obtained. The best performing nano-composite dope solution (7 wt. %) was then further treated for performance enhancement by increasing the water content to increase pore size and pore size distribution followed by coating with nano-fibres. The uncoated and coated flat sheets, were characterized by SEM, surface roughness, LEP_w and CAw. Flux analysis showed that the increase in water content had little effects on the VMD flux. It also suggests that; the nano-fibre layer posed very little resistance to mass transfer. A comparison of VMD and DCMD was also done experimentally.

Keywords: PVDF flat sheets, nano-fibre, Superhydrophobic SiO_2, sponge-like layer, vacuum membrane distillation, direct contact membrane distillation.

Résumé

Des membranes nano-composites ont été préparés à partir de poly (vinylidène) fluoriné (PVDF). La solution dopée contenait des concentrations variées de nano-particules superhydrophobes SiO2 . Les membranes fabriquées ont été caractérisées par SEM, FTIR, angle de contact, LEPw, rugosité de surface, diamètre des pores et distribution de la taille des pores. L'effet des nanoparticules sur la performance de la membrane a été ensuite analysée. Les membranes nano-composite ont démontré une augmentation de diamètre des pores sur la surface, un angle de contact plus élevées, et un plus petit LEPw par rapport aux membranes non-traitées. La membrane nano-composite contenant 7 ms% a démontré le plus grand flux sur le processus VMD, avec un flux de 2,9 kg / m2.h, représententant une augmentation de 4 fois par rapport à la membrane non-traitée. Des tests de dessalation ont aussi été réalisées. En utilisant une solution de sel contenant 35 g / L d'eau, le rejet de sel obtenu était de > 99,98%. La meilleure solution de nano-composite était de 7 ms% . Celle-ci a ensuite été traitée en augmentant ça teneur en eau, pour améliorer ses performances (taille des pores et la distribution de taille des pores). Les membranes ont ensuite été caractérisées par SEM, rugosité de surface, LEPw et TCA. L'analyse de flux a montré que l'augmentation de la teneur en eau a eu peu d'effets sur le VMD. Nous avons égallement vu que que la membrane ne résistait pas au transfert de masse. Une comparaison de VMD et de DCMD a également été fait déterminée expérimentalement.

Acknowledgment

I would like to express my special and sincere thanks and appreciations to my supervisor and co-supervisors Dr. Christopher Lan, Dr Takeshi Matsuura, and Dr. Dipak Rana. You have been tremendous mentors to me, guiding and providing me with all the necessary support. I would like to specifically thank you for encouraging my research and giving me the opportunity to grow as a research engineer. All your effort and dedication is priceless.

My gratitude also goes to the administrative and technical staff in the Department of Chemical and Biological Engineering, Faculty of Engineering at the University of Ottawa.

I also acknowledge the support of the Carleton University SEM lab through Dr. Jianqun Wang for their tremendous support with SEM analysis.

Arkema Inc. (Philadelphia, PA, USA) are also appreciated for their donation of the poly(vinylidene) fluoride, the base polymer for this study.

Special gratitude to all the members of our industrial membrane research group especially Mohammadali Baghbanzadeh and Yifan Yang for their inspirational support, friendship and togetherness showed to me all through the course of this work.

To my lovely daughters Kerry-Johnson and Margaret and lovely wife Sally for their unspeakable encouragement, perseverance and love they showed to me all the way through. Sincere thanks to my mother and grandmother and Miss Charlotte Mojoko for their spiritual support.

Finally, I am grateful to the Almighty GOD, through HIM wisdom, good health and love was showered to all the participants of this project to see it to an end.

Table of Contents

List of figures

List of tables

Legend

J	Transmembrane flux ($g/m^2.h$)
A	Membrane area (cm^2)
ρ	Density of the testing liquid (g/cm^3)
k_B	Boltzmann constant
k_m	Membrane thermal conductivity
$T_{f,m}$	Membrane surface temperature (feed side)
$T_{p,m}$	Membrane surface temperature (permeate side)
δ	Membrane thickness
ΔHv	Heat of vaporization
h_f	Heat transfer coefficient
ψ	Temperature polarization coefficient
C_m	Concentration at feed side membrane surface
C_f	Concentration of bulk
Φ	Concentration polarization coefficient
λ	Mean free path

k_n	Knudsen number
ε	Porosity
r_{max}	Maximum pore size

1 Introduction

The rise in clean water demand for domestic, agricultural and industrial purposes is becoming a more severe topic of debate in recent times. Several factors are driving the scarcity of clean water including human factors as well as climate changes. The most recent proof is the clean water rationing in the state of California, USA, where severe droughts were experienced forcing authorities to take measures in order to cut down water use for less important needs to provide for the most important once e.g. drinking. There is therefore no need to over emphasize the urgency to find alternative methods to provide clean water, since the problem is no longer an issue of the future but of the present. Several means of providing clean water to the population have been in use including treatment of already used water (wastewater) for re-consumption and desalination of saline and brackish water to drinkable water.

With 72% of the planet covered by saline water, oceanographers have stated that, 97% of the earth's water is saline water amounting to a total volume of 1.35 billion cubic kilometers. There is no doubt that desalination would provide a huge relief for this humanitarian crisis. Desalination technologies could be divided into;

- Thermal processes such as Multiple Effect Distillation (MED), and Mechanical Vapor Compression (VC)
- Membrane processes including Reverse Osmosis (RO), Forward Osmosis (FO), Ultrafiltration (UF), Microfiltration (MF), Nanofiltration (NF), and Membrane Distillation (MD)

Reports show that around 63.7% of the clean water produced from these desalination technologies is as a result of membrane-based processes with the remainder coming from thermal processes [1]. RO is being considered as the world's leading desalination process since 60% of pure water recovered from desalination comes from RO [2, 3]. That notwithstanding, RO faces drawbacks [1, 4]; fouling problems , a very concentrated retentate which poses environmental disposal risks, limited recovery (40-60%), very high electrical energy consumption required to pressurize the feed (3-4 kWh/m^3) and additional feed pre-treatment related costs. With all the potentials RO is posing, taking the above mentioned drawbacks into consideration; researchers have thus proceeded to look into other membrane processes such as MD.

MD is an emerging technology which is on the verge of overthrowing RO [3] with other great features like high quality of permeate at relatively high salt concentration of feed, milder operating conditions, possibility to use the low-grade heat sources, little or no feed pre-treatment required, minimal fouling and scaling tendencies since no pressure is applied.

1.1 The problem statement

With all the potentials that MD has shown, it is still not yet commercialized for large scale desalination purposes as is the case with RO. Though being so close to tackling most of the drawbacks, issues like membrane stability, fouling, flux stability and energy required for feed evaporation are still crowding the MD process making it relatively expensive to produce pure water by this means. Due to immense research work done by researchers in this domain, a better understanding of the process has been established both at the microscopic and macroscopic levels. For example, multi-effect MD configurations have been developed with heat recovery systems[4] thus limiting the need for high energy consumption and even processes that do not

require heating the feed. Researchers are now capable of controlling the flux through manoeuvring with the pore size and pore size distribution, liquid entry pressure of water (LEP_w) and others. Though MD is being used at the pilot scale for desalination, [5] for it to stand alongside RO, the cost per cubic meter of pure water produced by MD has to be less than that produced from its rivalling RO. For instance RO has been able to produce pure water at \$0.40/m^3 while MD is at around \$1.0/m^3. Al-Obaidani et al. [6] performed a cost analysis on a DCMD desalination system with a total capacity of 8500 tons/day. They concluded that the cost of pure water was \$1.17/m^3 and \$1.25/m^3 for a DCMD process with and without heat recovery, respectively. It is worthy to note that while most estimations regarding the costs of pure water via MD desalination were in the range of \$1 - \$2/m^3 [6], an impressive re-estimation showed that a lower cost of \$0.26/m^3 could be achieved if the thermal energy was obtained without any cost [3, 7]. For the cost to be kept at minimal, all of the setbacks outlined above have to be addressed squarely.

1.2 Thesis objectives

The aim of this work is to look into one of the drawbacks related to MD membranes; i.e. MD flux is not high enough. Though a lot of research work has been done in relation to this domain, the novelty of this project is the incorporation of nano materials into the polymeric MD membrane. More specifically, this work will aim at fabricating nano-composite membranes with the capability of the following;

- Generate a much higher and stable vapour flux over a period of time.
- Enhanced durability of the membrane with the aid of nano-fibre incorporation.

- Attain a high rejection at the highest achievable vapour flux.
- Achieve the highest flux with minimal heating of feed ($27^{o}C$).

To attain the set goals, superhydrophobic nano-silica particles will be incorporated into the polymer matrix of the membrane. The membranes shall further be coated with nano-fibre material and the performance tested against the untreated membrane.

2 Literature review

In the last decades, chemical engineers have sought for varying methods to improve the processes of separation and purification. These improvements are more or less specifically directed to curbing of the effects of one or more operating parameters of the process. Separation and purification techniques are one of the most involved processes in the downstream engineering procedures. Most of these techniques (Evaporation, distillation, filtration, reverse osmosis, etc) involve some kind of feed pre-treatment, or adjustments to process parameters. Though these techniques deliver the end results as required, they do so at the expense of one or more operating conditions (high temperatures or pressures) thus increasing the cost of the process: the driving force behind the need for a more cost effective technique.

One of the proven cost effective separation and purification technique is membrane distillation (MD) which has seen a substantial improvement from its time of conception. MD is capable of reducing the operating cost by using much less pressure (as opposed to pressure driven techniques like reverse osmosis, RO), at lower temperatures (as opposed to traditional evaporation). MD is a membrane based separation process that relies on vapour pressures difference (usually brought about by a temperature difference) across a suitable membrane. Since its conception in the late 1960s this membrane dependent process is yet to be commercialized

due to drawbacks posed by a suitable membrane that meets the characteristics required for the process.[9] These characteristics include;

- Porosity: The membrane should be porous with at least 60% porosity.
- Hydrophobicity: Process liquid should not be able to wet the membrane surface.
- Pore wetting: No capillary condensation should take place inside the pores of the membranes.
- Rejection: Only vapor should be capable of passing through the pores of the membrane and not process solutes.
- The membrane must not alter the vapor equilibrium of the different components in the process liquids.
- Flux: The highest attainable trans-membrane flux should be stable for the entire process.
- Fouling: the membrane should be less prone to fouling or scaling no matter the feed being treated.

2.1 Membrane distillation configurations

Several MD configurations have been employed in treating aqueous feed solutions using micro-porous hydrophobic membranes. Irrespective of which configuration is in use, the three regions of a typical setup will include a feed side, the membrane layer and the permeate side as shown in Fig. 2-1 below.

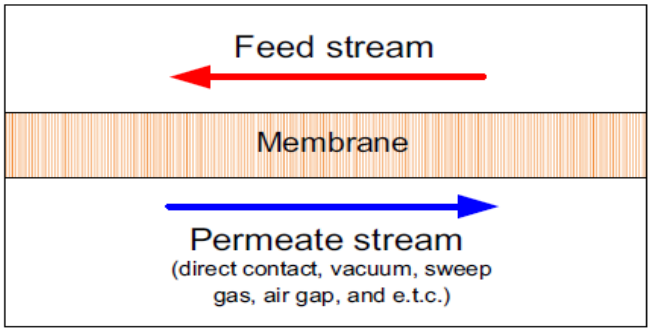

Figure 2-1. Illustration of the MD process [4]

Some of the MD configurations include;

2.1.1 Vacuum Membrane Distillation (VMD)

The schematic diagram of a VMD setup is shown in Fig. 2-2D. In this configuration, a vacuum pump is employed to generate vacuum in the permeate side of the module with condensation occurring outside of the module with negligible heat losses due to conduction, which is considered as an advantage in the processing of aqueous volatile solution.

2.1.2 Direct Contact Membrane Distillation (DCMD)

This configuration (Fig. 2-2A) requires a hot feed solution to be in direct contact with the top surface of the membrane, while cold water flows through the other side. The vapour pressure difference across the membrane drives the flow of vapour from the feed side through the micro pores of the membrane and condenses on the cold permeates side. Though this configuration is the simplest and most widely used in desalination and food industries, it suffers from severe heat losses by conduction.

2.1.3 Air Gap Membrane Distillation (AGMD)

The AGMD schematic is presented in Fig. 2-2B. Just as seen in the DCMD setup, the feed solution is in direct contact with the hot, top surface of the membrane. Air is then trapped between the membrane and the condensation surface. Vapour then travels across the air gap to condense on the cold surface inside of the membrane module. Though there is an additional resistance to mass transfer caused by this air gap, this configuration suffers less from heat losses due to conduction when compared to DCMD.

2.1.4 Sweeping Gas Membrane Distillation (SGMD)

As shown in the schematic diagram in Fig. 2-2C, SGMD uses an inert gas to sweep the vapour found at the permeate side of the membrane for condensation to take place outside of the membrane module. Un- like in AGMD where there is a stationary phase air barrier for reduction of heat losses, in SGMD the air (gas) is not stationary, a great enhancement factor to the mass transfer. This configuration, though very efficient in separation of volatile aqueous solutions, has as a main drawback the need for relatively large condensers since a very small volume of permeate is swept by a large volume of gas. To mitigate this problem of large condenser, AGMD and SGMD can be merged in a process known as thermostatic sweeping gas membrane distillation (TSGMD) where the inert gas passes through the gap between the membrane and the condensation plate. AGMD then occurs with some of the vapour condensing on the condensation surface and the remainder is swept by the gas to condense outside of the membrane module (SGMD).

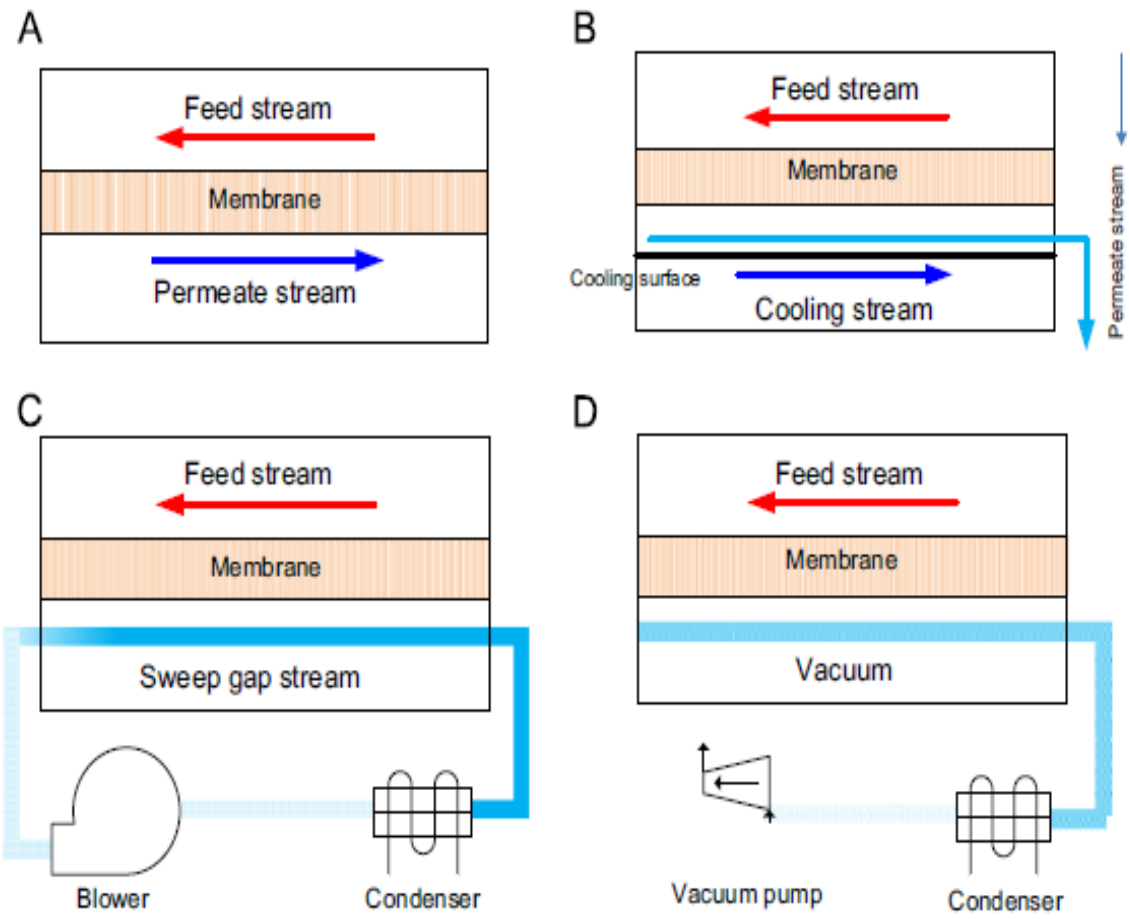

Figure 2-2. Basic MD configurations. A) DCMD, B) AGMD, C) SGMD, D) VMD [4]

2.2 MD membrane fabrication

Though membrane distillation was established in the 60s, till date the fabrication of an optimal membrane for the MD process is still an ongoing issue amongst researchers. Since the membrane must meet certain criteria as stated earlier, different polymers, solvents, additives and techniques have been used in the struggle to produce an optimal membrane. For the reason of being hydrophobic, the polymers used in membrane fabrication must have relatively low surface tension [4]. The table below shows some commonly used polymers and their surface tension.

Table 2-1. Major MD membrane polymers and their surface tensions

Polymer	Critical surface tension(dynes/cm)
Polyacrilonitril (PAN)	44
Polysulfon (PS)	41
Polyphenyloxide (PPO)	41
Polyethylene (PE)	31
Polytetrafluoroethylene (PTFE)	18.5
Polypropylene (PP)	29
Polyvinylidenefluoride (PVDF)	25-28.5
Fluorinated ethylene propylene (FEP)	16

The table shows that polymers like FEP would turn to produce more hydrophobic membranes while PAN will produce more hydrophilic membranes. But due to the complexity in the dissolution of the polymer, PVDF have been used more widely in producing MD membranes because of its chemical resistance, high thermal stability, ability to dissolve in most solvents and the mechanical strength of the membranes produced. Table 2-2 below shows the most commonly used solvents for dissolving polymers in membrane fabrication.

Table 2-2. Commonly used solvents and their boiling temperatures

Solvent	Boiling point (^{o}C)
N,N. Dimethhylacetamide (DMAc)	165
N,N. Dimethyformamide (DMF)	153
Dimethylsulfoxide (DMSO)	189
Tetrahydrofuran (THF)	65
Acetone	56.1

2.2.1 PVDF membrane preparation

Since this research was mainly focused around the use of PVDF for membrane fabrication, this section will provide a review of the preparation techniques. The preparation of PVDF membranes for MD has seen significant evolvement since its introduction in the 80s. Most of the commercial membranes are produced by phase inversion due to product flexibility, lower cost and simplicity. But other techniques like sintering and track etching have been successfully used and will also be discussed.

2.2.1.1 Phase inversion

In a polymer/solvent mixture, demixing is a common occurrence. The process by which the homogeneous polymer solution is transformed from its naturally occurring state of liquid to solid state could be described as phase inversion. The transformation process can be attained through more than one means including thermally induced phase separation (TIPS), vapour induced phase precipitation (VIPS), immersion precipitation (IP) and controlled evaporation of solvent

from three component systems. TIPS and IP are the two most widely used techniques in the fabrication of polymeric PVDF membranes.

Immersion precipitation is the most common and simplest of all the techniques where a polymer solution is cast on a support material usually with the use of a casting bar or rod and the support is usually a glass plate or backing material. The casted solution in then immersed in a non-solvent solution to enhance coagulation instigated as a result of the solvent exchange with the non-solvent. This technique favours PVDF membrane fabrication because of its ability to attain complete dissolution in most organic solvent as such the exchange is more effective. After coagulation, a semi-crystalline solid is formed with an asymmetric morphology. Researchers in the PVDF membrane field have studied the effects of different preparation conditions on the performance and morphology of the membrane. Kuo et al [42] changed the non-solvent from water to alcohol to produce superhydrophobic PVDF membranes while Yang et al [15] used water as the coagulation bath. Other conditions like temperature of the casting medium, the time of immersion in the coagulation, the solvent being used are all focus points in the attempt to optimize the process for better performing membranes.

Thermally induced phase separation (TIPS) unlike IP, is another common and useful technique in preparing MD polymeric membranes. In this process, a homogeneous solution comprising of a polymer dissolved in a solvent at high temperatures. Usually the solvent is of high boiling point and low molecular weight. The high temperature solution is then cast on a suitable support and allowed to cool. The cooling process induces phase separation and the polymer solidifies into a semi-crystalline membrane structure. The diluent is then removed to create a micro-porous membrane. Just like the exchange between the non-solvent and solvent which creates the phase separation in IP, TIPS involves the removal of thermal energy (heated to cooling) to transform the mixture into the two phases. In TIPS, the polymer crystallisation

process is highly dependent upon the diluents used. The crystallisation determines the membrane properties like morphology, pore size, mechanical strength, and even permeate flux. PVDF microporous membranes were produced through TIPS by using dibutyl phthalate as the diluents (Lloyd et al) [43]. The cooling and quenching conditions have also proven to affect the crystalline structure of the membrane. Sue et al [44] investigated the cooling rate and found that increasing the cooling rate decreased the crystallisation process.

2.2.1.2 Sintering

This is also another widely used technique in the production of commercial inorganic membranes. In this method, the powder polymer containing specified particle sizes are compressed and sintered at elevated temperatures without necessarily passing through a liquefaction stage. Porous PVDF membranes have been produced through sintering. Methyl isobutyl ketone (MIBK) was used to disperse PVDF powder and dispersion was then broken down into droplets which were then sintered at a specific temperature [45]. Glasrock Products Inc. and Solvay & Cie [45, 46], have successfully secured patent rights on the preparation of porous PVDF membranes by the sintering technique.

2.2.1.3 Track etching

This technique involves the use of high energy particle radiation (metal ions) to shape the surface of the polymer film to produce specific desired structures. This method has as advantage the ability to control the pore size, pore shape, porosity and pore size distribution of the film. In PVDF membrane track etching, the polymer film is exposed to the radiation particles applied perpendicular to the material surface thereafter which etching in an acid or alkaline bath follows [47]. Grasselli and Betz [48] irradiated PVDF film with heavy ions of Sn and the etched in permanganate oxide to produce membranes with pore diameters in the nanometer scale.

2.3 New MD configurations

Though MD can be operated at relatively low temperatures and ambient pressure when compared to RO and nanofiltration (NF), its low thermal efficiency has limited it from being commercialized. Hence rigorous works have thus been carried out to establish new MD configurations capable of overcoming the thermal barrier.

2.3.1 Multi-stage and multi-effect membrane distillation (MEMD)

Based on the concept of multi-stage and multi-effect distillation, an AGMD module was established with the capability of internal heat recovery (Fig 2-3). The cold feed solution is placed underneath the condensation plate to serve as coolant for permeate vapour to condense and at the same time gain heat. This allows for the pre-heated feed to be further heated before entering the feed chamber. A commercialized AGMD Memstil MD module is now available with great heat recovery potential. This module uses a micro-porous spiral wound PTFE membrane for seawater and brackish water desalination. DCMD modules with such potentials have been developed based on the same principles. These modules have reported significant low energy consumption (below 130kwh/m^3)[4].

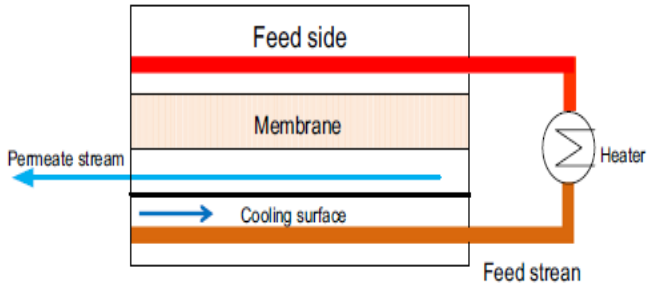

Figure 2-3. Illustration of AGMD with heat recovery system [4]

2.3.2 Multi-effect Vacuum Membrane Distillation (MEVMD)

The concept of multi-effect membrane distillation is the same as seen in MEMD but for the presence of an enhanced vacuum in MEVMD configuration (Fig. 2-4). A traditional MEVMD is made up of an external condenser, a heater and multiple evaporation-condensation units [10]. Vacuum is applied at the air gap space to remove excess air/vapor, allowing for the distillate produced to condense in each stage and inside the condenser. At each stage, the feed recovers the condensation heat and a multiple-effect phenomenon is generated. Commercial MEVMD configurations have been developed by Memsys with the use of PTFE membranes with average pore size of 0.2 microns for groundwater purification, brine concentration, solar driven desalination, and it is believed that the configuration showed a specific energy consumption of 175-350 kWh/m^3 [11, 12].

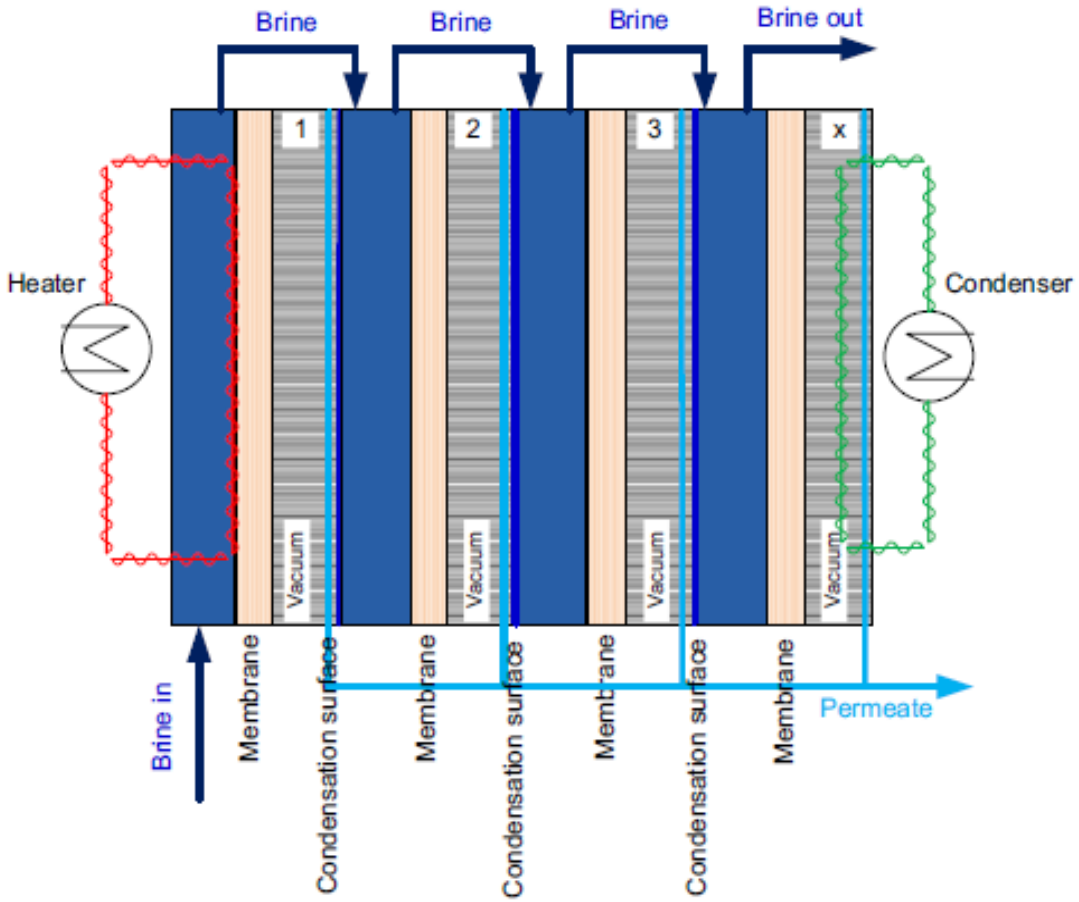

Figure 2-4. Illustration of MEVMD setup [4]

2.3.3 Material gap membrane distillation (MGMD)

AGMD usually shows a reduced permeation flux due to the presence of the stagnant air layer between the membrane and the condensation plate. This layer contributes greatly to resistance of mass transfer and therefore a new MD module was developed to overcome this resistance. In MGMD, the air gap is filled with different materials like Polypropylene mesh and sponge (polyurethane) [13]. By so doing, resistance to mass transfer could be greatly reduced and the permeation flux of up to 800% was achieved with MGMD systems.

2.4 Membrane Characteristics

For a membrane distillation module to be effective, an efficient membrane has to be available. MD membranes are hydrophobic (non-wetting), micro-porous and generally made from polymers with low surface energy like polytetrafluoroethylene (PTFE), polypropylene (PP) or polyvinyledineflouride (PVDF). These membranes turn to have low resistance to mass transfer, good thermal stability and low thermal conductivity to prevent trans-membrane heat losses and resistance to chemicals (acid and bases). MD membranes are thus characterized as follows;

2.4.1 Liquid entry pressure (LEP)

This characteristic also known as wetting pressure is of great importance since it determines the pressure at which the feed liquid penetrates into the membrane pores. The LEP of a membrane is highly dependent on its maximum pore size and the hydrophobicity of the membrane surface [14]. Since the main goal is separation of an aqueous solution, knowing the LEP will determine the pressure limit to achieve separation.

According to Franken et al. [14], LEP, ΔP can be determined from the Eq. 1 (Young- Laplace equation)

$$\Delta P = P_f - P_p = \frac{-2B\gamma_l \cos\theta}{r_{\max}} \qquad (1)$$

Where P_f and P_p are the hydraulic pressure on the feed and permeate side, B is a geometric pore coefficient (equal to 1 for cylindrical pores), γ_1 is the liquid surface tension, θ contact angle and r_{max} is the maximum pore size. From Eq. 1, it is clear that, the larger the maximum pore size, the lower the LEP, and the less suitable the membrane for MD purposes because of membrane

wetting. MD membranes should have LEP values of at least 3 bars [15], as a result membranes with high contact angle (high hydrophobicity) and small pore sizes turn to have high LEP values. [16]

2.4.2 Membrane thickness

One of the factors that pose great resistance to mass transfer in membranes is the membrane thickness. This significant membrane characteristics has an inversely proportional relationship with trans-membrane flux (flux reduces as membrane thickness increases). Since heat losses turn to reduce as the membrane thickness increases, Lagana et al [17] established that an optimal membrane thickness lies between 30-60 μm.

2.4.3 Membrane porosity

This refers to the void volume fraction of the membrane denoted by the pore volume with respect to the total membrane volume. It is known that, highly porous membranes are associated with larger flux due to larger evaporation surface area and lower conductive heat loss. Smolder-Franken [18] developed an equation to determine the porosity, Eq. 2.

$$\varepsilon = 1 - \frac{\rho_m}{\rho_{pol}} \tag{2}$$

where ρ_m and ρ_{pol} represents the density of membrane and polymer respectively. Membrane distillation membranes are expected to have a certain minimum porosity to be suitable for the process. El-Bourawi et al [19] established that the minimum MD membrane porosity lies around 30% with an upper limit of around 85%.

2.4.4 Mean pore size and pore size distribution

Pores are the channels for vapour transport hence the larger the pores, the higher the flux. Since all the pores are not the same, the mean pore size is used to determine the trans-membrane flux. Though a larger pore size is required for higher flux, the size should be small enough to avoid feed solution from penetrating into the membrane (wetting) as such an optimum pore size is required depending upon the operation conditions and the feed being treated. MD membrane pore sizes range between 100 nm to 1 μm [19]. Researchers have demonstrated varying opinions on the use of mean pore size and pore size distributions in the determination of permeate flux. Khayet et al [18] acknowledged the fact that, caution must be taken in the determination of vapour flux with use of mean pore size instead of pore size distribution.

2.4.5 Scanning Electron Microscopy (SEM)

The membrane geometry of the top surface, the cross-section and the bottom surface (see Fig. 2-5) are usually analysed using SEM images which have also been used in estimating the porosity, pore size, pore size distribution and membrane thickness [20]. SEM images are generated when a beam of high energy electrons hits the atoms on the surface of the sample (usually coated with gold), resulting in the release of low energy atoms from the sample which are then detected to produce a micrographic image.

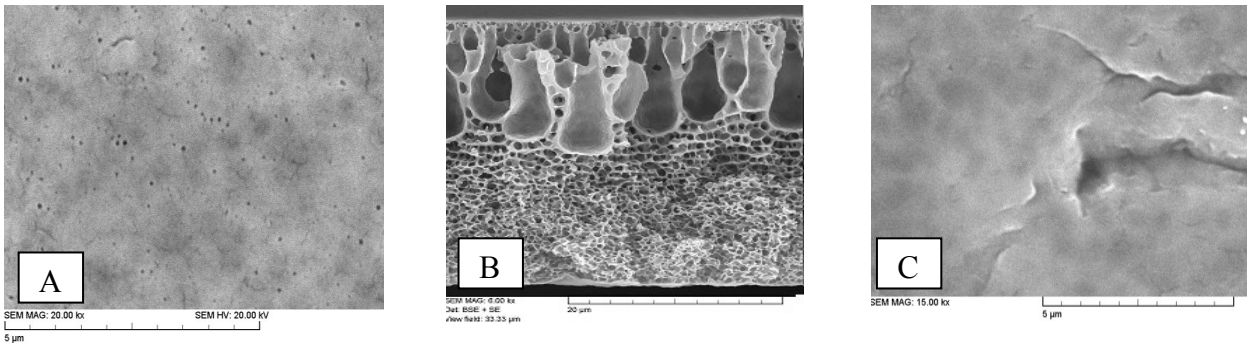

Figure 2-5. SEM images showing membrane geometry. A) Top, B) cross-sectio, C) Bottom

2.4.6 Atomic Force Microscopy (AFM)

The surface topography of MD membranes is usually analysed using AFM. The 3-D images generated (Fig. 2-6) show how rough the membrane surface is. The roughness parameters are calculated from AFM images by using a computer software built-in the AFM equipment. Roughness is most often related to contact angle; the rougher the surface, the higher the contact angle and thus the more hydrophobic the membrane [20]. Khayet et al [22] also used AFM to determine porosity, pore size, and pore size distribution.

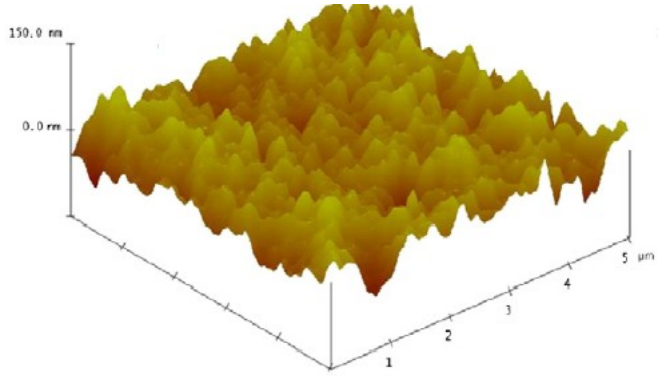

Figure 2-6. AFM image of membrane top surface

2.5 Applications of MD processes

2.5.1 Seawater/brackish water desalination

The rapid population growth and industrialization have placed the availability of potable drinkable water in jeopardy. As such more and more need for drinkable water is raising worldwide concerns, pushing researchers to develop new reliable processes like MD to address the situation. MD has been geared towards desalination of seawater but its application for brackish water desalination is gaining grounds within the industrial and academic milieu. Pilot desalination plants constructed based on commercialized MD systems [23] has successfully

produced pure drinkable water from saline water. Heat recovery designs of AGMD have been tested and used successfully [24, 25] and showed energy consumptions of 294 kwh/m^3. In Singapore and China, VMEMD Memsys systems have been tested with reliable results obtained [26].

2.5.2 Removal of small molecule contaminants

Since membrane technologies like RO and NF for wastewater treatment [27, 28] cannot effectively remove small molecule contaminants, MD with its capability of accomplishing high rejection of small molecules, is being highly considered for this purpose. In Asia and North America, wastewater usually contains some Boron compounds which have successfully been treated with up to 50% rejection using RO [29]. These Boron contaminants and other compounds like arsenic have been removed from wastewater using MD with a rejection >99.8%.

With the growth and expansion of the oil and gas sector worldwide, it is evident that the water surrounding the oil industries most likely suffers from spills. Oil-water separation is receiving attention worldwide as a result of this. Usually the oily water is treated by means of dissolved air flotation, skimming, de-emulsification and coagulation. These methods have proven to be less efficient for oily wastewater treatment [30, 31]. MD, with its ability to operate without any hydraulic pressure, is less susceptible to fouling, increasing the chances of MD as an efficient separation means for oily wastewater. A stable membrane performance was achieved using oily wastewater as feed for over 24 h when treated in a MD process with plasma-modified PVDF membranes [32]. A modified Memsys PTFE membrane (For oil resistance) system also showed high rejection with feed wastewater containing 0.1 wt. % oil. MD systems and operations have been employed for the treatment and removal of organic compounds such as ammonia, aromatic compounds and trichloroethane[33, 34].

2.5.3 Recovery of valuable components

MD varies from most of the other separation technologies because of its unique transport mechanism. The difference in vapour pressure and volatility of different components in a feed mixture makes MD capable of concentrating one component against the other, either in the feed or in the permeate stream. This principle has been applied in the concentration of fruit juices, sugar, alcohol herbal extracts and others [35, 36]. Feed mixtures containing water and a more volatile acid or alcohol have been separated using MD with the acid/alcohol being enriched in the permeate stream [37, 38]. In the metallurgy industry where large volumes of HCl are used, waste streams containing the volatile acid have been treated with MD processes to recover the acid in the permeate stream with purities high enough for direct recycling back into the process [39].

2.6 Mass transfer in MD

Mass transfer in MD includes three steps; Vaporization of liquid feed at the membrane interface, vapor molecules travel across membrane pores toward the cold interface as a result of vapor pressure differences, and finally, depending upon the MD configurations, vapor molecules would condense either in a liquid stream or carried away by a moving gas etc.

It therefore implies that mass transfer is dependent on two key factors: the ability of the membrane to allow vapor through it (membrane permeability) and the vapor pressure difference across the membrane (driving force). Applying the universal transport equation (3) for mass transfer through the membrane to correlate the mass flux to the vapor pressure difference across the membrane,

$$J = C_m(P_f - P_p) \tag{3}$$

Where C_m is membrane coefficient, J is flux, P_f and P_p are the vapor pressure at the membrane feed and permeate surfaces, respectively, estimated using the Antoine equation.

There are several points that should be considered in mass transfer through the membrane:

1. Since the porosity of a membrane is always less than 100%, the effective area for mass transfer is lower than that of the total area of the membrane.
2. Since the membrane pores do not go straight through the membrane, vapor molecules travel a greater path than the membrane thickness.
3. Resistance to diffusion increases by the inside walls of the pores due to a decrease in momentum of the vapor molecules.

Three basic mechanisms have been postulated for mass transfer: Knudsen diffusion (K), Poiseuille or viscous flow (P), Molecular diffusion (M) and the transition mechanism which is combination of the various mechanisms. In the Knudsen region the vapor molecules/pore wall collisions are dominant over molecule-molecule collision, while in molecular diffusion, the vapor molecules collide with each other, and a Knudsen/Molecular mechanism depicts that the vapor molecules collide with each other, and also diffuse through the air film. In Poiseuille flow (viscous flow), the gas molecules act as a continuous fluid driven by a pressure gradient [3]. To determine which mechanism is dominant in mass transfer across the membrane, a Knudsen number has to be computed as defined by the following equation:

$$Kn = \frac{\lambda}{d} \tag{4}$$

λ is the mean free path of the molecules (the average distance traveled by a molecule between consecutive collisions) and d is the mean pore size of the membrane. λ is obtained from the kinetic theory using the Eq. 5.

$$\lambda = \frac{k_B T}{\sqrt{2}\pi P d_e^2} \tag{5}$$

k_B, T and P are Boltzmann constant, absolute temperature, and average pressure within the membrane pores, respectively.

Kn is used to determine which mechanism of mass transfer is prevailing through the membrane for a given set of parameters. A high Kn value denotes that the mean free path of vapor molecules is large in comparison with the membrane mean pore size, while a lower Kn value shows that the membrane pores size is larger relatively.

2.7 Heat transfer in MD

Heat transfer just like mass transfer in MD has kept researchers continuously on the search for more information and understanding to improve the process. Heat transfer (Fig. 2-7) involves sensible heat and latent heat transfers through the membrane as a whole and through individual membrane pores.

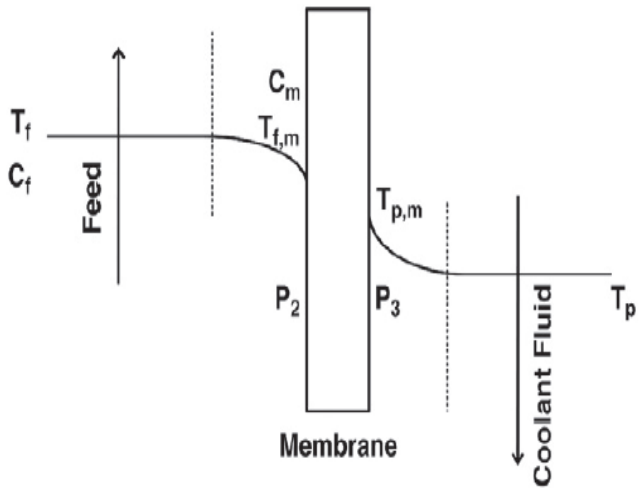

Figure 2-7. Heat transfer profile across a MD membrane

Since only vapor is expected to pass through the membrane pores, latent heat is carried by the vapor from the feed bulk side of the higher temperature to the permeate cold side of the lower temperature. But within the hot feed side, between the membrane surface and the bulk feed, a boundary layer is created through which heat is transferred by convection. Sensible heat transfer across the membrane is by means of conduction depending upon the thermal conductivity of the membrane. It therefore implies that both conduction and convection heat transfer mechanism are in and depending also on the MD configuration in question, these forces may act differently.

Quantitative analysis of the conduction and convection relationships follows;

Heat transfer via convection in the feed boundary layer:

$$Q_f = h_f (T_f - T_{f,m}) \tag{6}$$

Where h_f is heat transfer coefficient at the feed boundary layer.

Heat transfer across the membrane via conduction and vapor molecules movement:

$$Q_m = \frac{k_m}{\delta}(T_{f,m} - T_{p,m}) + J\Delta H_v \tag{7}$$

Where k_m, δ, J and ΔH_v are membrane thermal conductivity, membrane thickness, permeate flux and heat of vaporization, respectively.

At steady state, conduction and convection are in equilibrium.

$$Q_f = Q_m \qquad \rightarrow \qquad \frac{k_m}{\delta}(T_{f,m} - T_{p,m}) + J\Delta H_v = h_f (T_f - T_{f,m}) \tag{8}$$

The above correlations are employed for heat transfer analysis for all the MD configurations except VMD where heat conduction through the membrane is negligible due to presence of vacuum thus reducing the heat balance to Eq. 6.

Pertaining to heat transfer, surface temperatures of both sides of the membrane (feed, $T_{f,m}$ and permeate, $T_{p,m}$) have been studied extensively but researchers have not yet established a consistent model in estimating these values experimentally. Al-Sharif et al [40] have used computational fluid dynamic (CFD) codes to investigate membrane surface temperatures and thermal polarization effects of counter current DCMD systems. Am attempt was made by Tamburini et al to measure the membrane surface temperature employing the techniques based on the use of thermochromic liquid crystals (TLC) [41]. The TLC was incorporated at the hot feed side and after they were illuminated, images were recorded at different experimental intervals and conditions, which were further analysed for temperature distribution using MATLAB image processing toolbox.

Eq. 9 below gives a quantitative estimation for the membrane feed side temperature and permeate side temperatures respectively;

$$\begin{cases} T_{f,m} = T_f - \dfrac{J\Delta H_v + k_m (T_{f,m} - T_{p,m})/\delta_m}{h_f} \\ T_{p,m} = T_p - \dfrac{J\Delta H_v + k_m (T_{f,m} - T_{p,m})/\delta_m}{h_p} \end{cases} \tag{9}$$

2.8 Temperature and concentration polarization

In DCMD process, feed solution evaporates at the membrane hot surface and creates a heat transfer boundary layer in the hot side. As well, by condensing the vapor molecules on the other side, a permeate heat transfer boundary layer would be generated on the cold side. The presence of boundary layers causes a temperature difference between the liquid-vapor interfaces and bulk fluids a phenomenon known as temperature polarization. It is introduced by the following relation:

$$\psi = \frac{T_{m,f} - T_{m,p}}{T_f - T_p} \tag{13}$$

Temperature polarization is defined according to Eq. 14 for a VMD module [42]:

$$\psi = \frac{T_f - T_{m,f}}{T_f - T_p} \tag{14}$$

Actually, temperature polarization shows the effect of heat transfer boundary layers on the total heat transfer resistance of the system. It means by reducing the boundary layer resistances, the temperatures at the liquid-vapor interface and at the bulk fluids comes close together and ψ approaches unity. On the other hand, if the heat transfer is controlled by the boundary layer resistances, the system approaches a high degree of temperature polarization and ψ becomes zero. For a DCMD arrangement, ψ is within 0.4-0.7.[2]. It is worth noting that temperature polarization is more applicable at high concentrations of solute, high temperature and low feed velocity [41], where the boundary layer resistances is greater. Usually, by introducing turbulence and using spacer materials, temperature polarization could be minimized.

Concentration polarization is stated according to the Eq. 15 as the increase of solute concentration on the feed side membrane surface to the solute concentration of the bulk feed, denoted as Φ.

$$\Phi = \frac{C_m}{C_f} \tag{15}$$

Solute concentration on the membrane surface is obtained from the following equation [2]:

$$Cm = Cf \exp\left(\frac{J}{\rho K}\right) \tag{16}$$

where ρ and K are liquid density and mass transfer coefficient, respectively.

Since the accumulated solute on the membrane surface produces a diffusive flow back to the feed [2], in modeling purposes, concentration polarization and fouling should be taken into account, and vapor flux cannot be only estimated by Knudsen, molecular and Poiseuille flow mechanisms, due to the differences between the properties of boundary layer at the membrane surface and the bulk solution.

References

[1] N.Ghaffour, T. M. Missimer and G. L. Amy, Technical review and evaluation of the economics of water desalination: Current and future challenges for better water supply sustainability, *Desalination 309* (2013) 197-207

[2] Hassan, A. S., & Fath, H. E. S. Review and assessment of the newly developed MD for desalination processes. *Desalination and Water Treatment*, *51*(2013), 574-585.

[3] L.M. Camacho, L. Dumée, J. Zhang, J.-d. Li, M. Duke, J. Gomez, S. Gray, Advances in membrane distillation for water desalination and purification applications, *Water 5* (2013) 94–196.

[4] Wang, P., & Chung, T. Recent advances in membrane distillation processes: Membrane development, configuration design and application exploring. *Journal of Membrane Science, 474*(2015), 39-56

[5] A. Abdullah, D. Naif, H. Nidal. Membrane distillation: A comprehensive review. *Desalination 287* (2012) 2-18

[6] S. Al-Obaidani, E. Curcio, F. Macedonio, G. Di Profio, H. Al Hinai, E. Drioli, Potential of membrane distillation in seawater desalination: Thermal efficiency, sensitivity study and cost estimation, Journal of Membrane Science, 323 (2008) 85-98

[7] G.W. Meindersma, C.M. Guijt, A.B. de Haan, Desalination and water recycling by air gap membrane distillation, *Desalination 187* (2006) 291–301

[8] J.H. Hanemaaijer, J. van Medevoort, A.E. Jansen, C. Dotremont, E. van Sonsbeek, T. Yuan, L. De Ryck, Memstillmembrane distillation- a future desalination technology, *Desalination 199* (2006) 175–176.

[9] E. Drioli, A. Ali, F. Macedonio. Membrane distillation: Recent development and perspectives, *Desalination 356* (2015) 56-84.

[10] K. Zhao, W. Heinzl, M. Wenzel, S. Buttner, F. Bollen, G. Lange, S. Heinzl,N. Sarda, Experimental study of the memsys vacuum-multi-effect-mem- brane-distillation (V-MEMD) module, *Desalination 323* (2013) 150–160.

[11] R.B. Saffarini, E.K. Summers, H.A. Arafat, J.H. Lienhard V, Technical evaluation of stand-alone solar powered membrane distillation systems, *Desalination* 286 (2012) 332–341.

[12] ⟨http://www.genewscenter.com/Press-Releases/GE-and-memsys-Team-Up-to-Pursue-Water-Treatment-for-Unconventional-Resources-395d.aspx#downloads⟩

[13] L. Francis, N. Ghaffour, A. Alsaadi, L. Amy, Material gap membrane distillation: A new design for water vapor flux enhancement, *J. Membr Sci*, 448 (2013) 240-247

[14] A.C.M. Franken, et al., Wetting criteria for the applicability of membrane distilla- tion, *J. Membr. Sci. 33* (3) (1987) 315–328.

[15] Yang, Y., Rana, D., Matsuura, T., Zheng, S., & Lan, C. Q. (2014). Criteria for the selection of a support material to fabricate coated membranes for a life support device. *RSC Advances*, *4*(73), 38711–38717M. Alklaibi, N. Lior, Membrane-distillation desalination: status and potential, Desalination 171 (2) (2005) 111–131.

[16] F. Laganà, G. Barbieri, E. Drioli, Direct contact membrane distillation: modelling and concentration experiments, J. Membr. Sci. 166 (1) (2000) 1–11

[17] M. Khayet, T. Matsuura, Preparation and characterization of polyvinylidene fluoride membranes for membrane distillation, *Ind. Eng. Chem. Res. 40* (24) (2001) 5710–5718.

[18] M.S. El-Bourawi, et al., A framework for better understanding membrane distillation separation process, *J. Membr. Sci. 285* (1–2) (2006) 4–29.

[19] Khemakhem, R.B. Amar, Grafting of Fluoroalkylsilanes on Microfiltration Tuni- sian Clay Membrane, *Ceram. Int. (2011)* doi:10.1016/j.ceramin., 2011.04.128.

[20] M. Khayet, K.C. Khulbe, T. Matsuura, Characterization of membranes for mem- brane distillation by atomic force microscopy and estimation of their water vapor transfer coefficients in vacuum membrane distillation process, *J. Membr. Sci. 238* (1–2) (2004) 199–211.

[21] M. Khayet, A. Velázquez, J.I. Mengual, Modelling mass transport through a po- rous partition: effect of pore size distribution, *J. Non-Equilib. Thermodyn 29* (3) (2004) 279–299.

[22] R.B. Saffarini, E.K. Summers, H.A. Arafat, J.H. Lienhard V, Technical evaluation of stand-alone solar powered membrane distillation systems, *Desalination* 286 (2012) 332–341.

[23] H. Lu, J.C. Walton, A.H.P. Swift, Desalination coupled with salinity-gradient solar ponds, *Desalination 136* (2001) 13–23.

[24] Scarab development solution to fabrication plant, in: Water Desalination Report, 2000

[25] Memsys secures a second pilot study, in: Global Water Intelligence, 2011, pp. 29

[26] D. Van Halem, S.A. Bakker, G.L. Amy, J.C. Van Dijk, Arsenic in drinking water: A worldwide water quality concern for water supply companies, Drinking Water *Engineering and Science 2* (2009) 29–34.

[27] A. Criscuoli, E. Rossi, F. Cofone, E. Drioli, Boron removal by membrane contactors: The water that purifies water, Clean Technologies and Environ- mental Policy 12 (2010) 53–61.

[28] K.L. Tu, L.D. Nghiem, A.R. Chivas, Boron removal by reverse osmosis membranes in seawater desalination applications, *Separation an*d Purification *Technology 75* (2010) 87–101.

[29] M. Stewart, K. Arnold, Emulsions and oil treating equipment-selection, sizing and troubleshooting, Gulf Professional Publishing, 2008.

[30] M. Gryta, K. Karakulski, The application of membrane distillation for the concentration of oil-water emulsions, *Desalination 121* (1999) 23–29.

[31] G. Zuo, R. Wang, Novel membrane surface modification to enhance anti-oil fouling property for membrane distillation application, Journal of Membrane Science 447 (2013) 26–35.

[32] L. Zhang, L.Xie, J.M. Shen, H.L. Chen, Effects of operation conditions on vacuum membrane distillation performance for epoxy resin wastewater, in: The 231st ACS national meeting, Atlanta, GA, USA, 2006.

[33] B. Wu, X. Tan, W.K. Teo, K. Li, Removal of benzene/toluene from water by vacuum membrane distillation in a PVDF hollow fiber membrane module, *Separation Science and Technology 40* (2005) 2679–2695.

[34] M. Tomaszewska, M. Gryta, A.W. Morawski, Study on the concentration of acids by membrane distillation, *Journal of Membrane Science 102* (1995) 113–122.

[35] T. Mohammadi, O. Bakhteyari, Concentration of L-lysine monohydrochloride (L-lysine-HCl) syrup using vacuum membrane distillation, *Desalination 200* (2006) 591–594.

[36] R. Thiruvenkatachari, M. Manickam, T.O. Kwon, I.S. Moon, J.W. Kim, Separa- tion of water and nitric acid with porous hydrophobic membrane by air gap membrane distillation (AGMD), S*eparation Science and Technology 41* (2006) 3187–3199.

[37] Z.L. Xie, T. Duong, M. Hoang, C. Nguyen, B. Bolto, Ammonia removal by sweep gas membrane distillation, *Water Research 43* (2009) 1693–1699.

[38] M. Tomaszewska, M. Gryta, A.W. Morawski, Mass transfer of HCl and H2O across the hydrophobic membrane during membrane distillation, Journal of Membrane Science 166 (2000) 149–157.

[39] S. Al-Sharif, M. Albeirutty, A. Cipollina, G. Micale, Modelling flow and heat transfer in spacer-filled membrane distillation channels using open source CFD code, *Desalination 311* (2013) 103-112.

[40] A. Tamburini, P. Pitò, a. Cipollina, G. Micale, M. Ciofalo, A thermochromic liquid crystals image analysis technique to investigate temperature polarization in spacer-filled channels for membrane distillation, *J. Membr. Sci. 447* (Nov. 2013) 260–273.

[41] L.F. Greenlee, D.F. Lawler, B.D. Freeman, B. Marrot, P. Moulin, Reverse osmosis desalination: water sources, technology, and today´s challenges: a review, *Water Res. 43* (2009) 2317–2348.

[42] Kuo, C., Lin, H., Tsai, H., Wang, D., & Lai, J. (2008). Fabrication of a high hydrophobic PVDF membrane via nonsolvent induced phase separation. *Desalination, 233*(1-3), 40–47.

[43] D.R. Lloyd, K.E. Kinzer, H.S. Tseng, Microporous membrane formation via ther-mally induced phase separation. I. Solid–liquid phase separation, Journal of Membrane Science 52 (3) (1990) 239–261

[44] Y. Su, C. Chen, Y. Li, J. Li, PVDF membrane formation via thermally induced phase separation, Journal of Macromolecular Science, Part A: Pure and Applied Chemistry 44 (1) (2007) 99–104

[45] C.A. Dickey and J.E. Mcdaniel, Method of producing spherical thermoplastic particles,

U.S. Pat. 3,896,196 (1975).

[46] P. Georlette, J. Leva, Composition comprising a vinylidene fluoride polymer and a blowing agent, U.S. Pat. 4,425,443, (1984).

[47] M. Mulder, Basic Principles of Membrane Technology, Kluwer Academic Pub-lishers, 1996.

[48] M. Grasselli, N. Betz, Making porous membranes by chemical etching of heavy-ion tracks in [beta]-PVDF films, Nuclear Instruments and Methods in Physics Research Section B: Beam Interactions with Materials and Atoms 236 (1–4) (2005) 501–507.

3 Effects of superhydrophobic SiO_2 nanoparticles on the performance of PVDF flat sheet membranes for vacuum membrane distillation

J.E. Efome et al., Effects of superhydrophobic SiO_2 nanoparticles on the performance of PVDF flat sheet membranes for vacuum membrane distillation, *Desalination* (2015). doi:10.1016/j.desal.2015.07.002

ABSTRACT

Polyvinylidene fluoride (PVDF)/SiO_2 flat sheet composite membranes were prepared for vacuum membrane distillation (VMD) by the phase inversion immersion precipitation process. The effect of blending superhydrophobic SiO_2 nanoparticles into the PVDF dope solution was studied. The concentration of the nanoparticles in the dope solution was varied at different wt. % (1, 2, 4, 6, 7, 8 and 10 wt. %). The prepared membranes were characterized by scanning electron microscopy, water contact angle, porosity, liquid entry pressure of water, Fourier transformed infrared spectroscopy, and VMD at feed temperature of 27°C. The nanoparticles enhanced the membrane performance through a reduction in the sponge-like layer thickness and an increase in surface pore size, leading to increased vapour flux with a maximum at 7 wt. %. The salt rejection was greater than 99.98% when a 35 g/L NaCl solution was used as feed. At this concentration, the smallest thickness of the sponge-like layer and largest macro-voids were also achieved. Beyond 7 wt. %, the sponge-like layer became predominant and the flux was reduced. With a vapour flux increase of up to 4 times (from 0.7 to 2.9 kg/m^2 h) when compared to the neat membrane, this nanocomposite membrane could be of great potential in the desalination process through VMD.

Keywords: Polyvinylidene fluoride (PVDF), superhydrophobic SiO_2 nanoparticles, sponge-like layer thickness, vacuum membrane distillation (VMD).

3.1 Introduction

The demand for drinkable water is showing an increasing trend due to the rise in global population. The total amount of water on earth is believed to be constant that goes through a re-cycling process. Though 70% of the earth is covered by water, only 2.5% is fresh water, the rest being saline and ocean based [1]. With the increasing effects of global temperature rise (climate changes), surface water is suffering from constant evaporation creating more shortage of potable water and making the saline water more saline. The situation does not seem to be improving along with difficult challenges associated with controlling global warming and pollution [1]. Since there has not been a cost effective means to circumvent the crisis, global health, economic growth and even social welfare are at risk.

It is therefore imperative that other means of fresh water is required to meet the rising population demand such as desalination of sea water to potable water. Several conventional processes like ultrafiltration (UF), microfiltration (MF) reverse osmosis (RO) and multistage vacuum evaporation have been employed for water treatment but an emerging separation technique is needed [2]. Membrane distillation (MD) is proving to be more efficient than other processes because of: (i) Lower operating pressure than RO, (ii) Close to 100% salt rejection, (iii) Lower energy consumption than multistage evaporation, and (iv) Lower operating temperature. MD has been used for different applications such as in the food industry, environmental protection and pharmaceuticals. In MD the driving force is the difference in vapour pressure across the micro-porous membrane created by the temperature gradient across the membrane [2].

Following extensive research on MD [3-31], different configurations have been analysed: vacuum membrane distillation (VMD), air gap membrane distillation (AGMD), direct contact membrane distillation (DCMD) and sweep gas membrane distillation (SGMD) [6, 9]. Irrespective of which configuration is being applied, a membrane which meets specific characteristics is always employed to carry out the separation process. In all MD configurations, one of the membrane characteristics is hydrophobicity which determines the wettability of the membrane surface. Hydrophobic membranes do not get wet easily, hence allowing only water vapour and not liquid to pass through the pores at pressures lower than the liquid entry pressure (LEP_w). At pressures greater than the LEP_w, the micro-pores become wet and part of the feed solution seeps onto the permeate side, thus allowing for no separation [3, 4, 8]. Researchers have used several polymers in preparing hydrophobic membranes because these polymers have presented low surface energies, high chemical resistance, thermal stability, and good mechanical strengths. These polymers include; polyvinylidine fluoride (PVDF), polypropylene (PP), polyethylene (PE) and polytetrafluoroethylene (PTFE) amongst which PVDF is the most widely used [27, 28]. Several techniques of membrane preparation have also been investigated in preparing membrane distillation membranes. These include; thermally induced phase separation (TIPS), immersion precipitations, vapour induced precipitation (VIP), and air casting of polymer solution, all of which involve some kind of solvent for polymer dissolution. The most widely used solvents for PVDF membrane preparation are dimethysulfoxide (DMSO), dimethyformamide (DMF), and dimethylacetylamide (DMAc) which are capable of completely dissolving the polymer at moderate temperatures [6, 9, 27, 28].

In the last decade of research in MD, scientists have placed special focus on the hydrophobicity of the developed membranes because an efficient MD process must result in reliable flux measurements and consistent conductivity readings of the resulting permeate. As

such researchers have developed several means of achieving hydrophobic (water contact angle greater than 90°) and even superhydrophobic (contact angle greater than 130°) membrane surfaces [9]. Kuo et al. [16] obtained novel composite membranes by using alcohol as the coagulation agent through the phase invasion precipitation method. The membranes where reported to have contact angles greater than 130°. Razmjou et al. [24] fabricated hydrophobic membranes by coating the PVDF surface with TiO_2 which resulted in membranes with contact angles greater than 130°.

Recent research works have also included techniques to enhance the porosity, flux, and mechanical strength of the membranes. A blend of high and low molecular weight PVDF was used by Chen et al. [5, 6] to prepare flat sheet membranes of high porosity and improved LEP_w. Fontananova et al. [12] prepared membranes from PVDF copolymer (PVDF-co-hexafluoropropylene) and PVDF homopolymer. The copolymer membranes posed greater resistance to mass transport than the homopolymer due to a bi-layer formed at the top and bottom surfaces of the membrane. High porosity membranes where made by Khayet and Matsuura [14] using water as a pore forming agent. Wang and Chung [29] produced a mixed matrix hollow fibre membrane with high flux and porosity by adding hydrophobic clay particles into the dope. Other researchers have used a blend of polymers for the dope solution preparation. Yang et al. [32] fabricated membranes on support materials which were shown to enhance the flux by up to 15 fold when compared to the unsupported membrane.

The present research was carried out to fabricate hydrophobic PVDF/nanoparticles flat sheet composite membranes using superhydrophobic SiO_2 nanoparticles as additives. The hydrophobic porous membranes where prepared by the phase inversion precipitation method using deionised water as the nonsolvent additive and DMAc as the solvent. The membrane properties were

investigated at different concentrations of the nanoparticles. They were characterized by scanning electron microscopy (SEM), VMD, porosity, liquid entry pressure of water (LEP_w), and water contact angle. The rejection of the membranes was also tested for desalination by using synthetic salt water.

3.2 Experimental materials and method

3.2.1 Material

Poly(vinylidene) fluoride (PVDF) polymer of two different molecular weights: Kynar® 740 and Kynar® HSV 900 was supplied as resins powder from Arkema Inc., Philadelphia, PA. PVDF exists in the α, β, and γ phases. However, Kynar is mostly in the α phase [6] and the structure of PVDF is presented in the graphical abstract. Dimethyl acetamide (DMAc, > 99%) used as solvent was supplied by Sigma Aldrich Inc., St. Louis, MO. The pore forming agent and coagulation agent employed were deionised water (conductivity < 10 μS/m) produced by Millipore Q BIOCEL unit, Millipore, Billerica, MA. Superhydrophobic silica nanoparticles (purity: ≥ 99.8, particle size: 10-20 nm, surface area: 100-140 m^2/g), surface modified with single layer organic chains were supplied by SkySpring Nanomaterials Inc. (Houston, TX). Butan-1-ol (> 99.8%) was from Sigma Aldrich Inc., St. Louis, MO.

3.2.2 Preparation of dope solution

The dope solution was prepared by mixing PVDF (15 wt. %), DMAc (83.75 wt. %) and water (1.25 wt. %) together at a stirrer rotation of 180 rpm and 50°C for 72 h to ensure complete polymer dissolution and solution homogeneity. The solution was then allowed to de-gas for 24 h at room temperature. The required amount of nanoparticles was then added to the required

quantity of dope solution and the suspension was stirred at 100 rpm for 2 h to yield the dope solution with expected final wt. % (1, 2, 4, 6, 7, 8, and 10) of nanoparticles. Hereafter ‘‘nanoparticles concentration’’ means the nanoparticle concentration in the dope. The compositions for the respective concentrations are listed in Table 3-1.

3.2.3 Membrane casting method

The dope solution containing the nanoparticle at the desired wt. % was then cast on a glass plate using a casting bar (0.25 mm thickness) at a speed of approximately 7 cm s^{-1}. The plate was then exposed to air for 10-15 s, followed by immersion into deionised water at ambient temperature. Upon completion of phase inversion, the solidified polymer sheet was peeled off the plate, transferred into fresh deionised water at ambient temperature and kept there for 24 h. Thereafter, the sheet was allowed to dry at room temperature for 24 h. The dried membranes were then subjected to characterization.

Table 3-1. Composition of the dope solution for flat-sheet composite membrane preparation.

Membrane Code	**Dope solution concentration**			**Nanoparticles concentration in the dope suspension***
	PVDF (wt. %)	DMAc (wt. %)	Water (wt. %)	SiO_2 (wt. %)
MS-0	15	83.75	1.25	0.0
MS-1	15	83.75	1.25	1.0
MS-2	15	83.75	1.25	2.0
MS-4	15	83.75	1.25	4.0
MS-6	15	83.75	1.25	6.0
MS-7	15	83.75	1.25	7.0
MS-8	15	83.75	1.25	8.0
MS-10	15	83.75	1.25	10.0

*Dope solution was prepared before addition of nanoparticles. So the nanoparticles wt. % is relative to dope solution.

3.2.4 Characterization of dope solution (viscosity measurement)

Viscosity measurement was carried out with the aid of a rotational rheometer (Brookfield, Synchro-Lectric viscometer model: LVF). The solution to be analysed was poured into the testing valves and a suitable spindle connected and immersed into the solution. A suitable motor speed was selected and the spindle was allowed to rotate for 5-7 minutes until the monitor on the dial attained a constant value. The viscosity was calculated according to the rotation speed, spindle factor, and rotation factor. Three measurements per solution were performed and the average was reported.

3.3 Membrane characterization

3.3.1 Scanning electron microscopy (SEM)

The top surface and cross-sectional images were taken using a SEM system (Tescan, Vega-II XMU with Oxford Inca Energy 250X EDS). After being immersed in liquid nitrogen to embrittle, the membrane sample was broken and fixed on a metal holder using a conductive tape. The sample was then sputtered with a conductive metal (Gold, >99.8%) coating under vacuum. The coating instrument employed was Anatech Hummer VII. SEM images were then taken at randomly selected locations and at suitable magnifications.

3.3.2 Liquid entry pressure of water (LEP_w) measurements

The LEP_w of the membranes was measured using the setup shown in Fig. 3-1, and the following approach [10]. A static liquid reservoir was installed with a membrane sample of surface area 13.1 cm^2 and filled with 200 ml of deionised water at ambient temperature.

Compressed nitrogen from a cylinder was used to apply pressure on the liquid and a regulator was used to control the increment at 2 psi per 10 min until water dripped off continuously from the cell outlet. A pressure gauge connected on the line displayed the operating pressure. For each membrane, three samples were analysed and the average was reported. The pressure at which water was seen dripping off the cell was noted as the LEP_w.

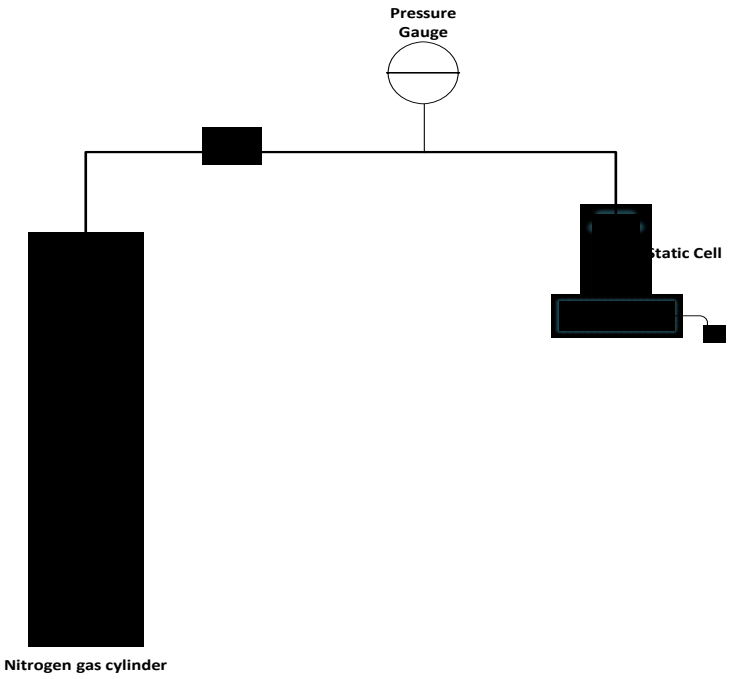

Figure 3-1. Schematic diagram of the experimental LEPw set-up.

3.3.3 Water contact angle measurements

The surface of each membrane was analysed for its hydrophobicity by measuring the water contact angle using a VCA Optima surface Analysis system (AST Products Inc., Billerica, MA). A 1 μL water droplet was dropped on the membrane surface using a micro syringe (Hamilton Company, Reno, NV) followed by a 10 s wait period, and then the angle was measured. Measurements were taken from 8 randomly selected spots and the average was reported.

3.3.4 Membrane surface roughness

The top surface of flat sheet membranes was analysed for roughness. A well suited software ImageJ was employed for the analysis. The SEM images were converted to a 32 bits image and an inbuilt plugin of ImageJ (*SurfCharJ*) could read the 7.5 µm x 7.5 µm size images to determine the roughness by computing the root mean square roughness (R_q) and the average roughness (R_a).

3.3.5 Energy Dispersive X-ray Spectroscopy (EDX) Analyses

To investigate how the nanoparticles are dispersed within the flat-sheet membranes, EDX analysis of the membrane cross-section was conducted using an Oxford Inca Energy 250X EDX apparatus.

3.3.6 Porosity and pore size measurements.

Three pieces were cut from randomly selected spots of a membrane sheet (area, 0.001884 m^2) and subjected to porosity measurements [21] using butan-1-ol. The pieces of membrane were kept immersed in a petri-dish that contained butanol for 24 h. They were then blotted, weighed and oven dried at 50°C for 24 h, followed by weighing again after drying. The porosity was calculated using the equation below and the average value was reported.

$$\% \varepsilon = \frac{m1-m2}{\rho.A.l} \text{x} 100\% \quad (1)$$

Where ε is the porosity (%), m_1 (g) is the weight of the wet membrane, m_2 (g) is the weight of the dry membrane, ρ (g/L) is the liquid density (butan-1-ol), A (m^2) is the effective surface area of the membrane, and l (m) is the membrane thickness measured using a micrometer.

Pore size measurement of the flat sheet membranes was carried out by applying the imageJ software on the top SEM image. Approximately 100 pores were randomly selected from the image and the average value was reported.

3.3.7 Vacuum membrane distillation (VMD)

VMD experiments were carried out to evaluate the performance of the composite membranes. The setup used for VMD is shown in Fig. 3-2 following a previous research work [5, 6]. The module consisted of a feed chamber with a permeation base where the membrane (0.113 m^2) was placed. A vacuum pump was used to apply vacuum (94.8 kPa) on the permeate side so that the permeated water vapour could be collected. The feed chamber was maintained at 27°C with the use of a heating coil connected to a temperature controller and kept under agitation to minimise temperature polarization effects. The procedure involved a 1 h pre-treatment by which air and moisture were sucked out of the lines. By doing so, the system was allowed to reach a steady state. All cold traps were cooled with liquid nitrogen. After the permeate vapour was collected in cold trap 3 during the 1 h pre-treatment, the vacuum line was switched to cold trap 2 where the permeate vapour was collected to measure the flux. Cold trap 1 was installed to prevent the oil contamination of the vacuum pump. The experiment was conducted for a predetermined time and the flux calculated using equation 2.

$$\text{Flux} = \frac{w}{t.A} \tag{2}$$

Where w (g) is the weight of condensate, t (h) is the time of flux collection, A (m^2) is the effective membrane surface area.

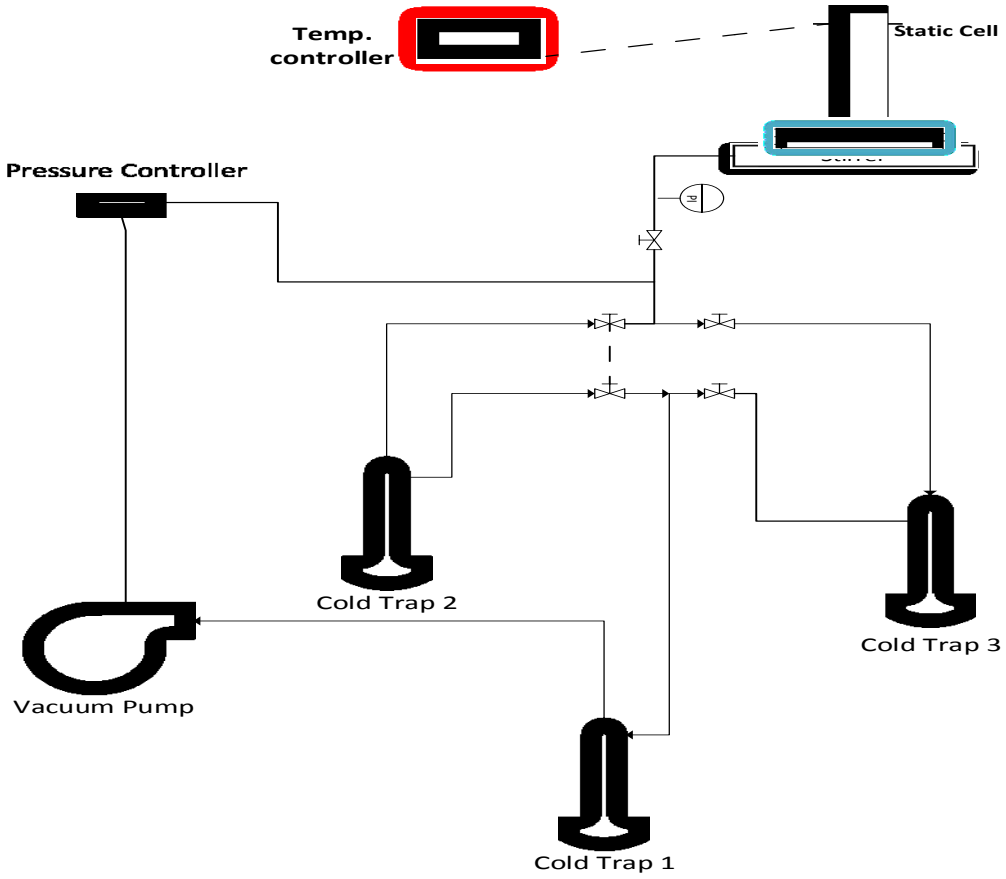

Figure 3-2. Schematic diagram of VMD set-up.

3.3.8 ATR-FTIR analyses

The prepared membranes were subjected to attenuated total reflectance (ATR) - Fourier transformed infrared spectroscopy (FTIR) spectroscopy by the Agilent tech-Cary630 (Agilent, Canada) spectrometer equipped with a diamond sampling accessory. The surface of the dried membranes were analysed by pressing and fixing the sample on the prism, and the IR spectra were recorded at 4 cm^{-1} resolution in the range of 650-3000 cm^{-1} with 64 scans.

3.3.9 Nanoparticle characterization (TEM)

The nanoparticles characterization was done to check for particle shape and surface properties (presence of pores). Transmission electron microscopy (TEM) (FEI Tecnai G2 F20 equipped with Oxford Aztec TEM with 80 mm SDD detector) was applied to observe the nano-structure of the silica nanoparticles. Samples were prepared by dispersing super hydrophobic silica powder into methanol. A drop of methanol was used for the dispersion of the nanoparticles on carbon-coated copper grids operating at 300 kV.

3.4 Results and discussion

3.4.1 Dope solution viscosity

Fig. 3-3 shows the results of viscosity measurements done at room temperature. It clearly illustrates a drastic increase in viscosity as nanoparticle concentration increases. Thus solvent/nonsolvent exchange rate is significantly lowered at high nanoparticle concentration. It is worth noting that the viscosity of the dope solution increased from 3.2 Pa.s of SM-0 (without blending nanoparticles) to 15 Pa.s of SM-10 (nanoparticles concentration 10 wt. %).

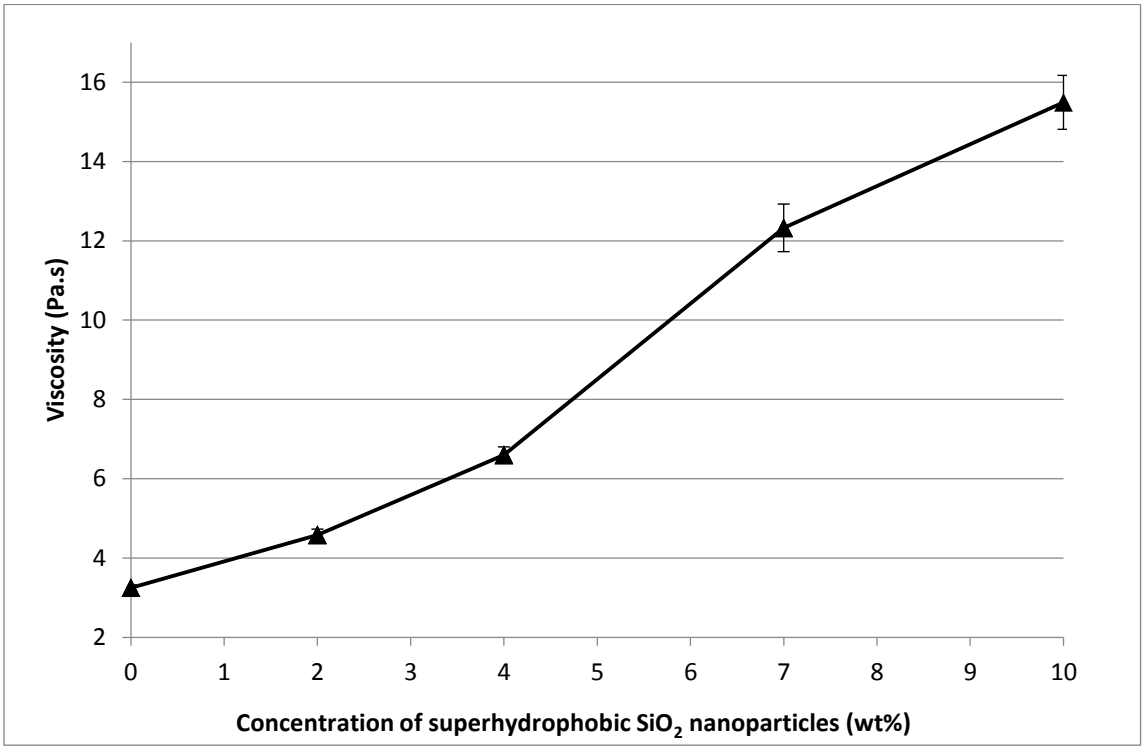

Figure 3-3. Viscosity measurements of the polymer solution.

3.4.2 Membrane characterization

3.4.2.1 Scanning electron microscopy (SEM)

To investigate the morphological changes associated with the addition of SiO_2 nanoparticles, SEM images of the top (T), cross-section (C) and bottom (B) of the membranes were taken as shown in Fig. 3-4. From the cross-sectional images, it is seen that the membranes have an asymmetric structure with a thin top skin layer, a finger-like macro-voids region, and a lower sponge-like layer. The effect of blending SiO_2 nanoparticles in the dope solution can be visually appreciated as a drastic change in the morphology is seen in the nanocomposite membranes (SM-4, SM-7, SM-10) when compared to the neat PVDF membrane (SM-0).

The top surface of the nanocomposite membranes presents a typical micro-porous surface showing a larger pore diameter but fewer in number than the neat PVDF membrane. Pores are formed by the phase inversion process. Demixing (presence of two phases; the polymer rich phase responsible for the solid continuous region and the phase with lesser polymer carrying the pore forming agents) plays a key role in pore formation. The higher the rate of demixing the lesser the appearance of the two phases, implying lesser pores will be formed [4-7].

Since water is the nonsolvent coagulation media and the SiO_2 nanoparticles are superhydrophobic in nature and disperse well in the dope solution, water molecules are compelled to come together during solvent/nonsolvent exchange to form larger droplets forming pores of larger sizes. Hence, the pore size increases upon addition of SiO_2 nanoparticles. Further increase in the nanoparticles concentration is supposed to increase the pore size progressively but the SEM images shows that the average pore sizes are approximately the same irrespective of concentration increase. This is ascribed to the weakened effect of hydrophobic nanoparticles as a result of their agglomeration.

As the SiO_2 nanoparticles concentration increases from MS-0-C to MS-10-C, a drastic change in the cross-sectional morphology is noticed. The membranes show a denser structure with smaller finger-like macro-voids. The finger-like layer disappears gradually, making it difficult to differentiate the finger-like layer from the sponge-like layer. This observation indicates that nanoparticles have a significant effect in the morphology of the membranes. During the solvent/nonsolvent exchange process, the increased viscosity caused by increase in nanoparticles concentration (see Fig. 3-3), poses greater resistance to the diffusion, resulting in the formation of fewer macro-voids but longer in depth [5-7, 11]. This shows that at concentration > 10 wt. %, the membrane loses its asymmetric morphology, adapting to a more

symmetric morphology made up primarily of the sponge-like layer and very dense. It is noted that the flux of the hydrophilic CuO nanoparticles incorporated PVDF composite membranes which increases with increasing concentration of nanoparticles due to the enlarging of surface pores and thickening the finger-like layer [33].

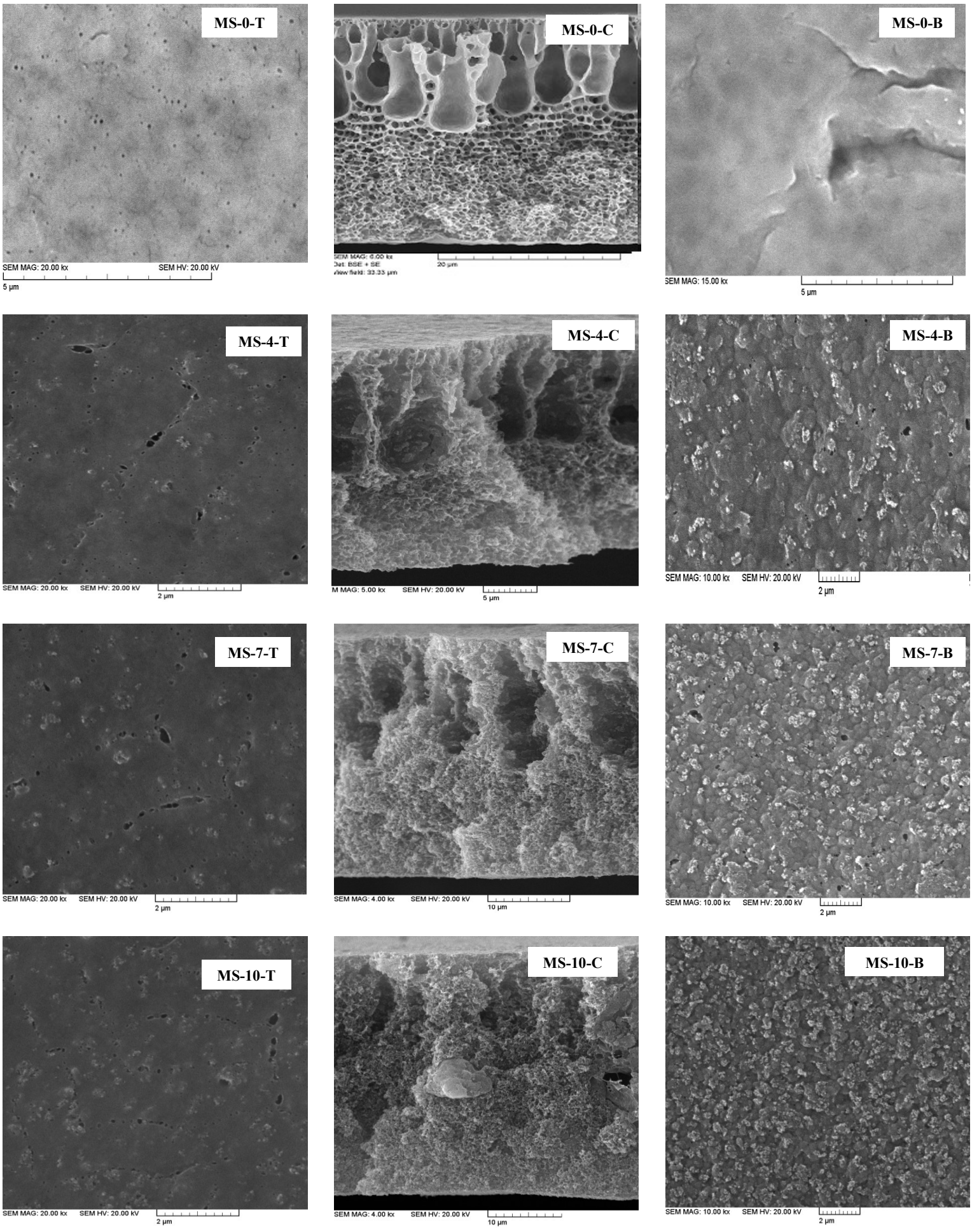

Figure 3-4. SEM images of the PVDF flat sheet nanocomposite membranes: T for top surface, C for cross-section, B for bottom surface.

3.4.2.2 LEP_w, Porosity and pore size measurements

VMD membranes are supposed to be able to support pressures of at least 3.0 bars [27, 31] to prevent water from fully penetrating the pores and disrupting the separation process. The experimental data for LEP_w is presented in Fig. 3-5. The results show that all PVDF-SiO_2 blended membranes have values above 45 psi (3.1 bar) with the maximum shown at nanoparticles concentration of 10 wt. %, it can thus be concluded that these membranes are suitable for VMD processes.

The decrease in LEP_w from the neat PVDF to the nanocomposite membrane is tentatively attributed to the increase in the surface pore size but amongst the nanocomposite membranes, the LEP_w value maintains an increase due to the decrease in membrane porosity with an increase in nanoparticles concentration.

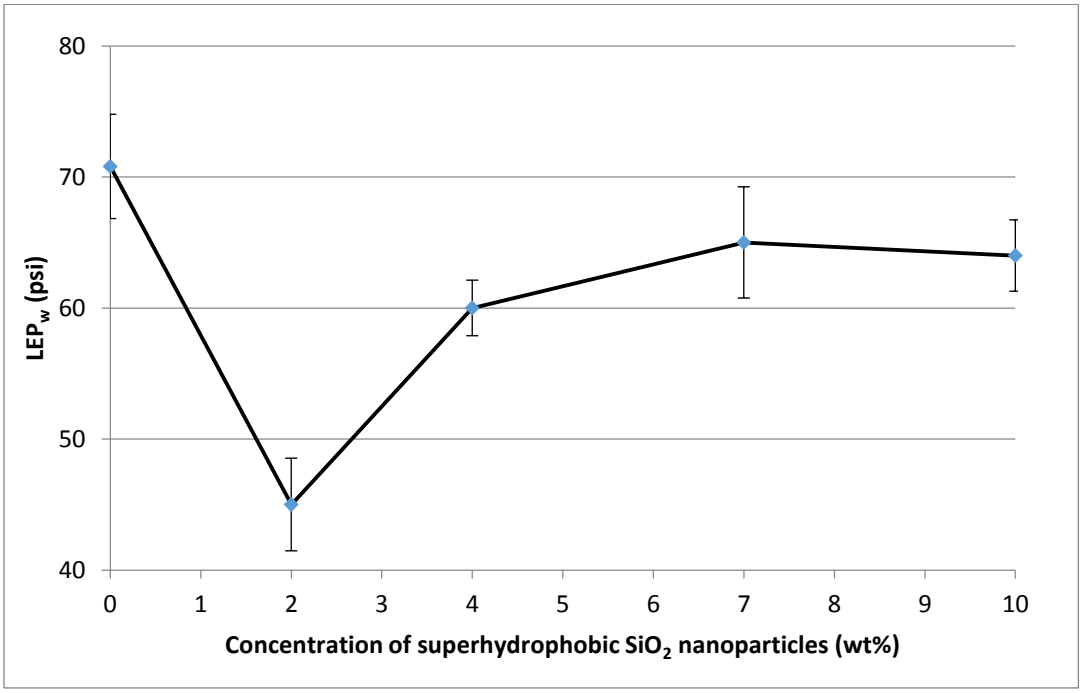

Figure 3-5. Effect of nanoparticles concentration on LEPw.

This further supports the fact that the surface pore sizes did not experience a great change amongst the blended membranes because if it did, the LEP_w would have seen a drop also caused by increased pore size.

The effect of the nanoparticle concentration on porosity is shown on Fig. 3-6. The neat membrane presented the highest porosity value >85% and the minimum value below 50% were shown at the nanoparticle concentration of 10 wt. %.

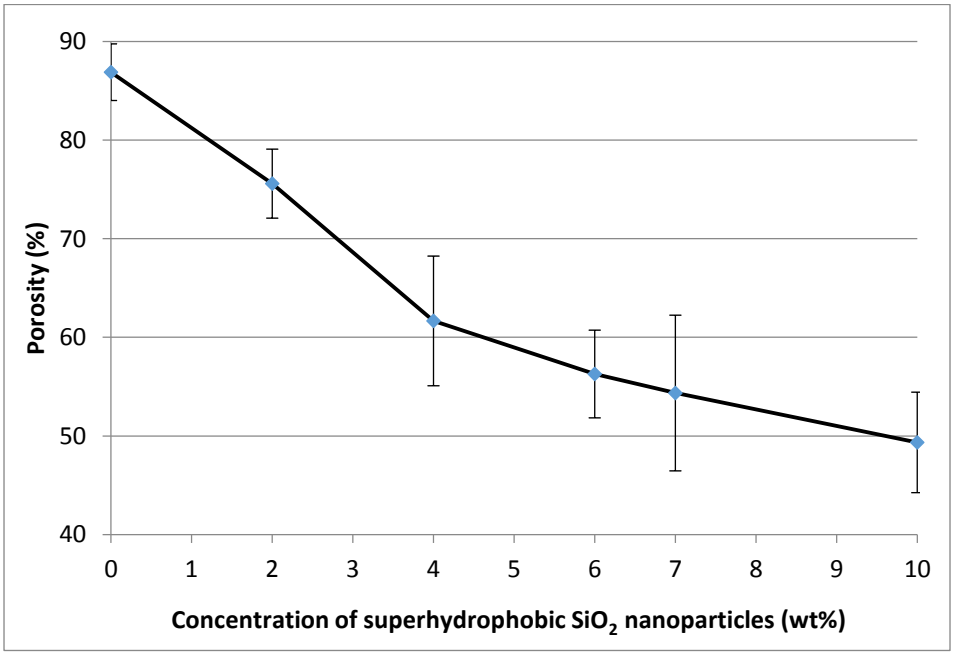

Figure 3-6.Effect of nanoparticles concentration on porosity.

This decrease in porosity ties with the increase in viscosity [7, 11] which caused the membrane to lose most of the finger-like layer and produced a denser sponge-like layer. The

SEM images of MS-4-C, MS-7-C and MS-10-C also confirm this phenomenon. The increase in the membrane dense nature reduces the size of micro-voids hence the porosity drops.

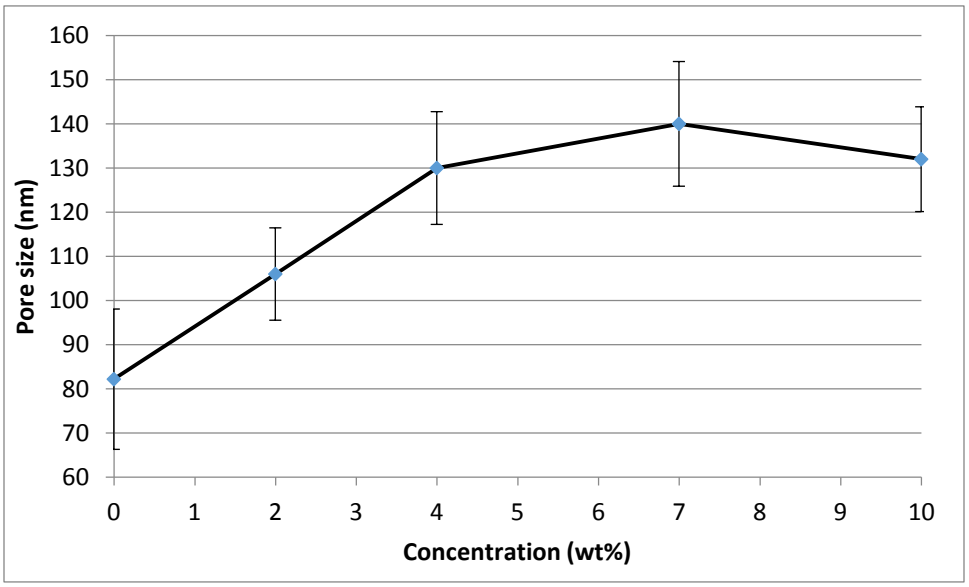

Figure 3-7.Effects of nanoparticles concentration on surface pore diameter.

Fig. 3-7 shows the pore size at the surface on the prepared membranes. As expected from the SEM top surface images (MS-0-T, MS-4-T, MS-7-T, MS-10-T), the pore size increases from nanoparticles concentration of 0 to 4 wt. % before levelling off.

3.4.3 Membrane surface properties

3.4.3.1 Water contact angle

The results of the water contact angle measurements are presented in Fig. 3-8. Since the nanoparticles used were superhydrophobic in nature, it was expected to increase the hydrophobicity of the nanocomposite membranes to near superhydrophobic levels. Though a superhydrophobic surface was not obtained, the hydrophobicity was enhanced. All

nanocomposite membranes showed values greater than the neat PVDF membrane, with the maximum contact angle attained (94°) at the nanoparticle concentration of 10 wt. %.

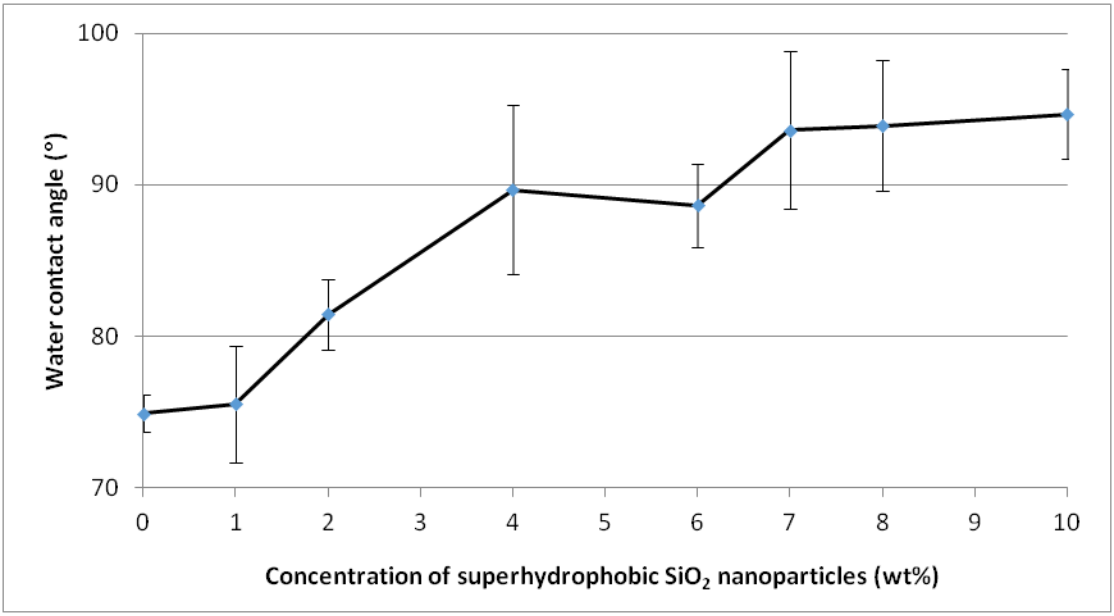

Figure 3-8. Effect of nanoparticles concentration on water contact angle.

It should be noted that, the contact angle of the dense composite membrane prepared by complete solvent evaporation showed significantly higher values than the corresponding porous membrane. For example, dense membrane that corresponds to MS-10 demonstrated features of a superhydrophobic surface with a contact angle >135°. This disparity in contact angle measurements could be explained by the fact that the dense membrane surface roughness is greater than the porous membrane [15-17] as a result of nanoparticles being exposed close to the surface.

3.4.3.2 Roughness analysis

Roughness parameters were obtained from the SEM top surface images using the *SurfCharJ* plugin of ImageJ software and the results shown in Table 3-2. The average roughness (R_a) defines the arithmetic average of the absolute values of the measured peak heights from a one dimensional plane, the root mean square (R_q) refers to the standard deviation and R_p denotes the maximum profile peak height. ImageJ surface analysis of the surface is shown in Fig. 3-9.

Table 3-2. Roughness parameters of the prepared PVDF nanocomposite flat sheet membranes.

Membrane code	R_a	R_q	R_p
MS-0	15.53	19.65	242
MS-4	27.88	50.58	255
MS-7	28.03	52.19	255
MS-10	27.28	49.35	255

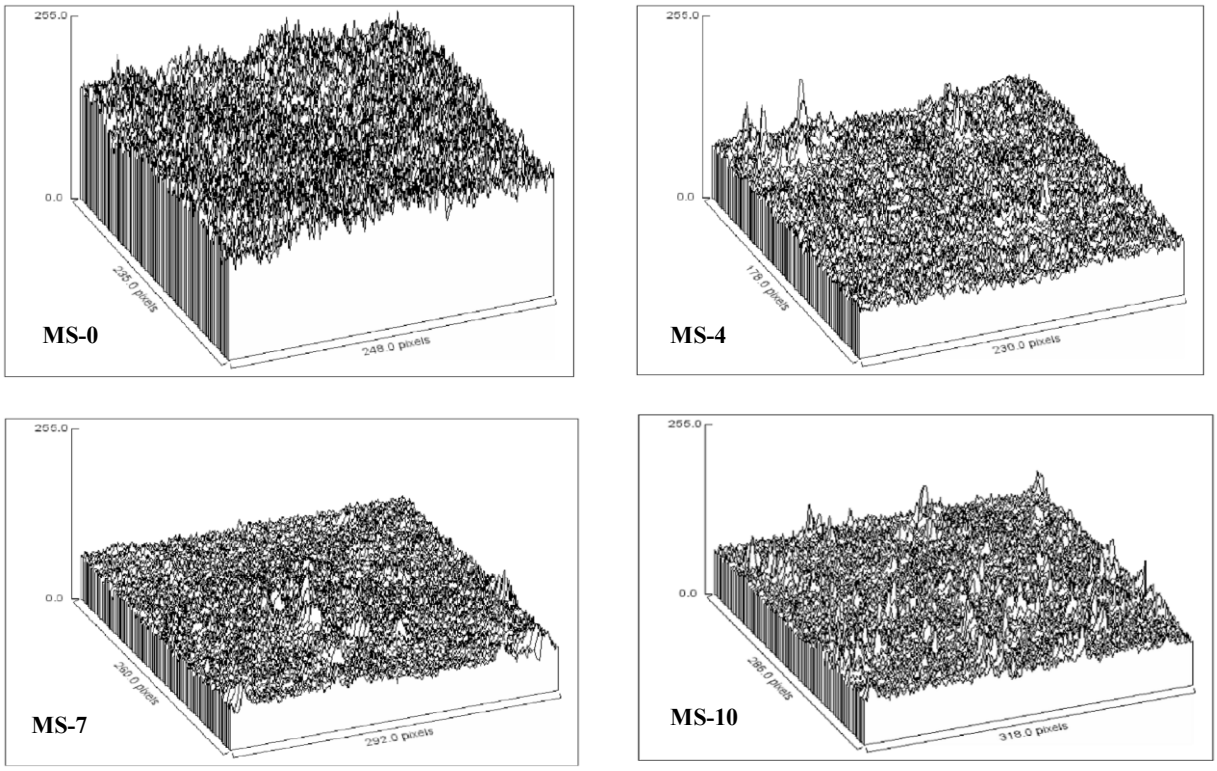

Figure 3-9. Three dimensional topographic images of neat PVDF and PVDF-SiO2 nanocomposite membranes.

It can be seen from the results that, the MS-0 membrane (neat PVDF membrane) had the smoothest surface with a R_a of 15.53 nm when compared to MS-4, MS-7, and MS-10 nanocomposite membranes. Amongst the nanocomposite membranes, there is not significant variation in the roughness parameters. This ties with the minimal variation in the water contact angle values seen amongst the nanocomposite membranes (Fig. 3-8). It is thus evident that the presence of the nanoparticles increased the surface roughness [11, 15], which led to an increase in the contact angle.

3.4.4 Particle distribution (EDX analyses)

Silicon mapping was performed across the cross-section of the nanocomposite membrane MS-2 and MS-7 to check for nanoparticle distribution and agglomeration as seen in Fig. 3-10.

Fluorine mapping is also shown in Fig. 3-10 since PVDF was the base polymer and fluorine should be seen all across the cross-section. From the figure, it is seen that the nanoparticles are distributed with little or no agglomeration across the cross-section since clusters of colours are not observed. The greater intensity of the coloration seen in MS-7 denotes an increase in concentration from 2 to 7 wt. % nanoparticles.

According to Fig. 3-11, three regions of the cross-section of MS-4 and MS-7 nanocomposite membranes were subjected to EDX. A section close to the top thin layer, the middle section and a section close to the bottom were sampled. It could be seen that, the nanoparticles dispersed uniformly throughout the cross section as shown by nearly equal Si peaks at the different locations. Detailed analysis of the wt. % of silicon at these locations has shown that its concentration reduces very slightly from the top to bottom. This could be due to the difference in densities between the nanoparticles and the polymer solution

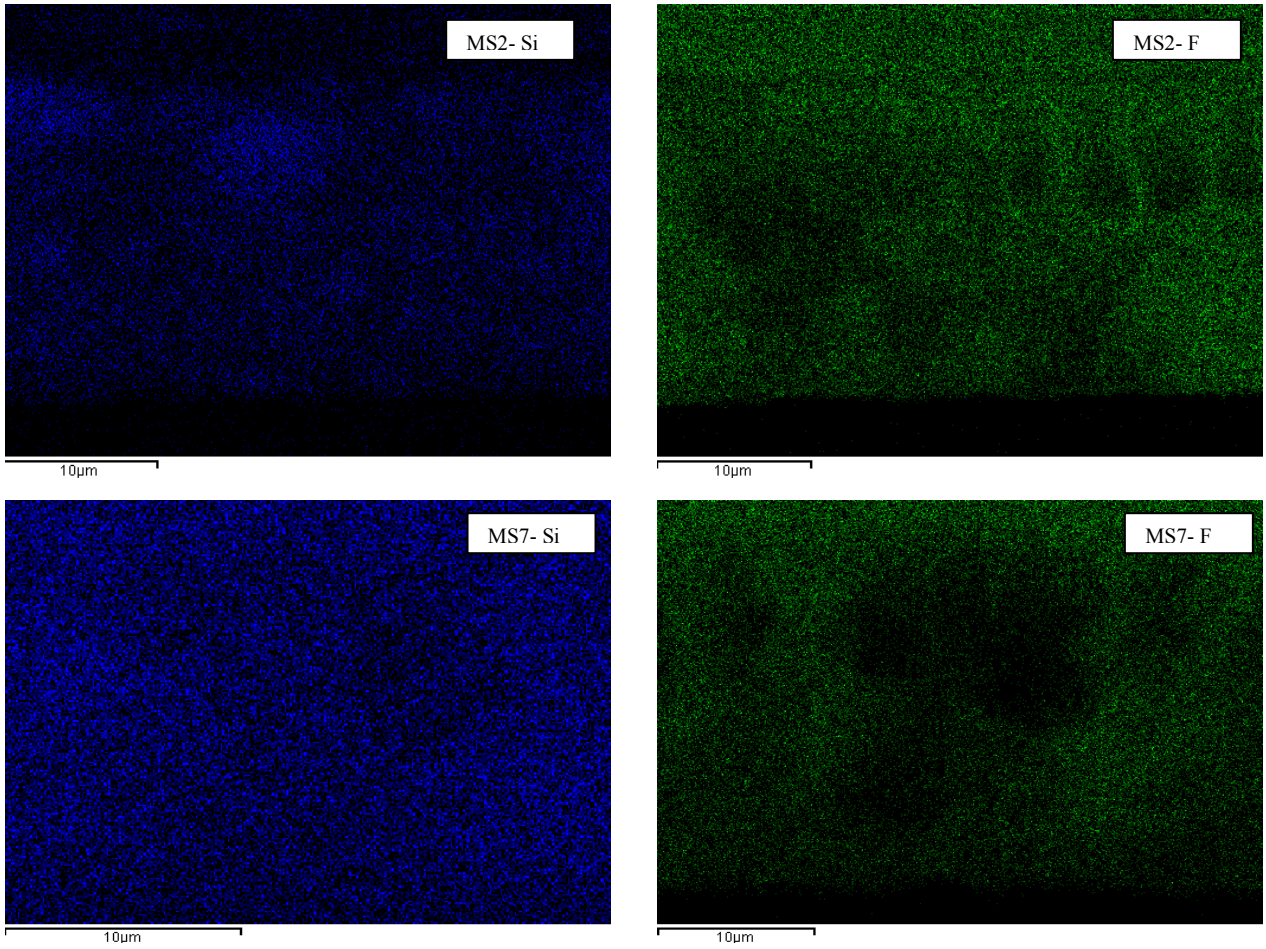

Figure 3-10. Silicon (Si) and Fluorine (F) mapping of PVDF-SiO2 nanocomposite membranes cross-sections.

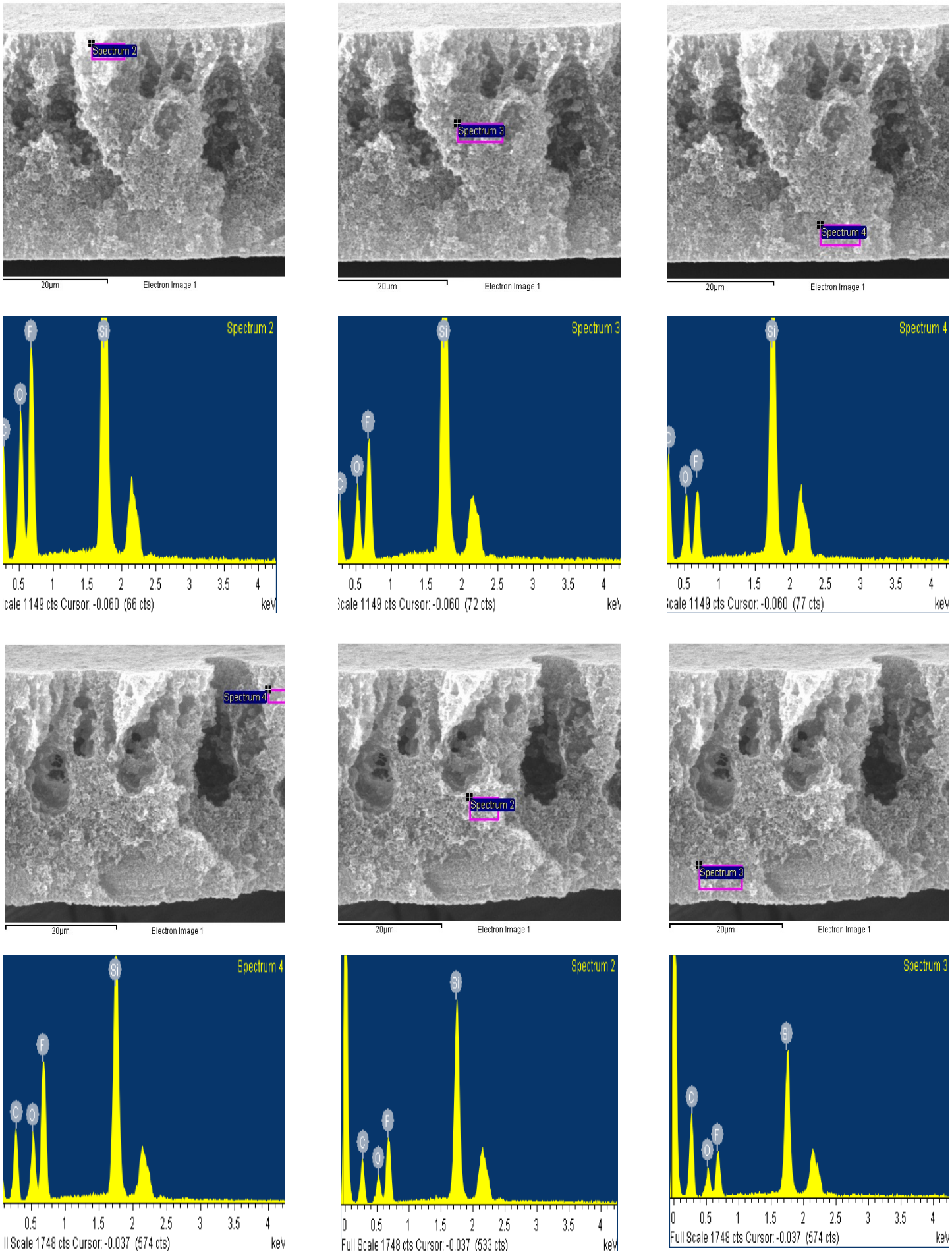

Figure 3-11. EDX images of flat sheet PVDF-SiO_2 nanocomposite membranes: MS-4 (first row) and MS-7 (third row).

3.4.5 ATR-FTIR analyses

The ATR-FTIR spectra of the prepared membranes with varying nanoparticles concentrations are presented in Fig. 3-12. PVDF being a semi-crystalline polymer has five possible polymorphs alternating between α-β transition states. All the membrane samples showed main absorption peaks at 840, 880, 1070, 1180 and 1400 cm^{-1} wave number, indicating that the PVDF polymer is made up of the α and β crystals [12, 24]. Since both crystals are present, it demonstrates that the phase inversion precipitation process did not create any chemical changes in the crystalline structure of the polymer.

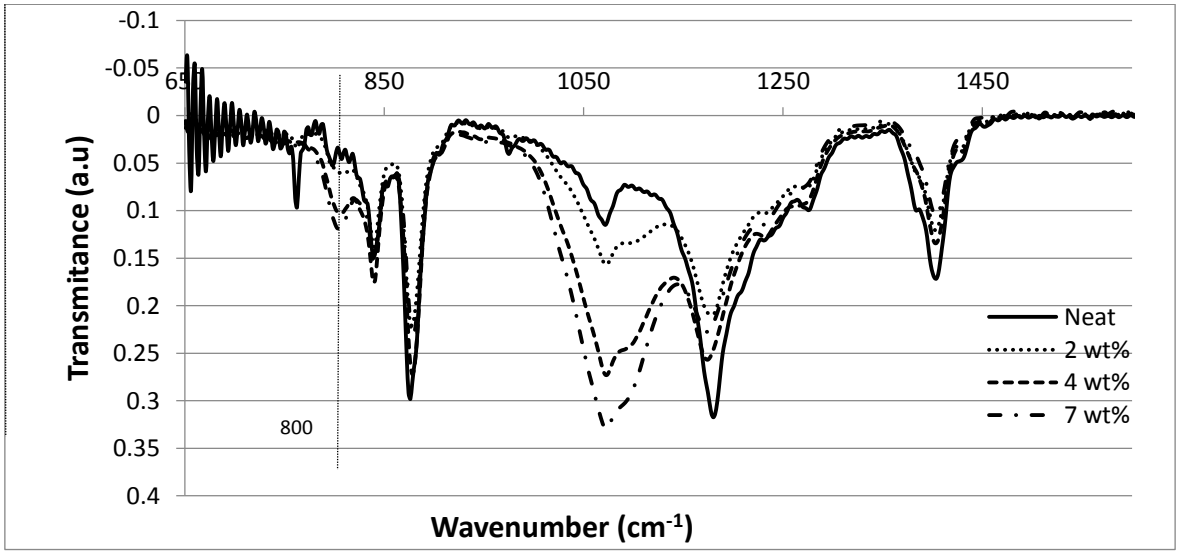

Figure 3-12. FTIR spectra of the neat PVDF (MS-0), 2 wt. % SiO_2-PVDF (MS-2), 4 wt. % SiO_2-PVDF (MS-4) and 7 wt. % SiO_2-PVDF (MS-7) nanocomposite membranes.

The appearance of an absorbance peak at 800 cm^{-1}, a characteristic SiO_2 peak suggests the inclusion of nanoparticles in the membrane.

3.4.6 TEM analysis

Fig. 3-13 shows the nanoparticles TEM images of particle shape and diameter. From the results, it could be seen that, the nanoparticles are near spherical and have diameters ranging from 10-20 nm which are compatible with the specifics provided by the manufacturer.

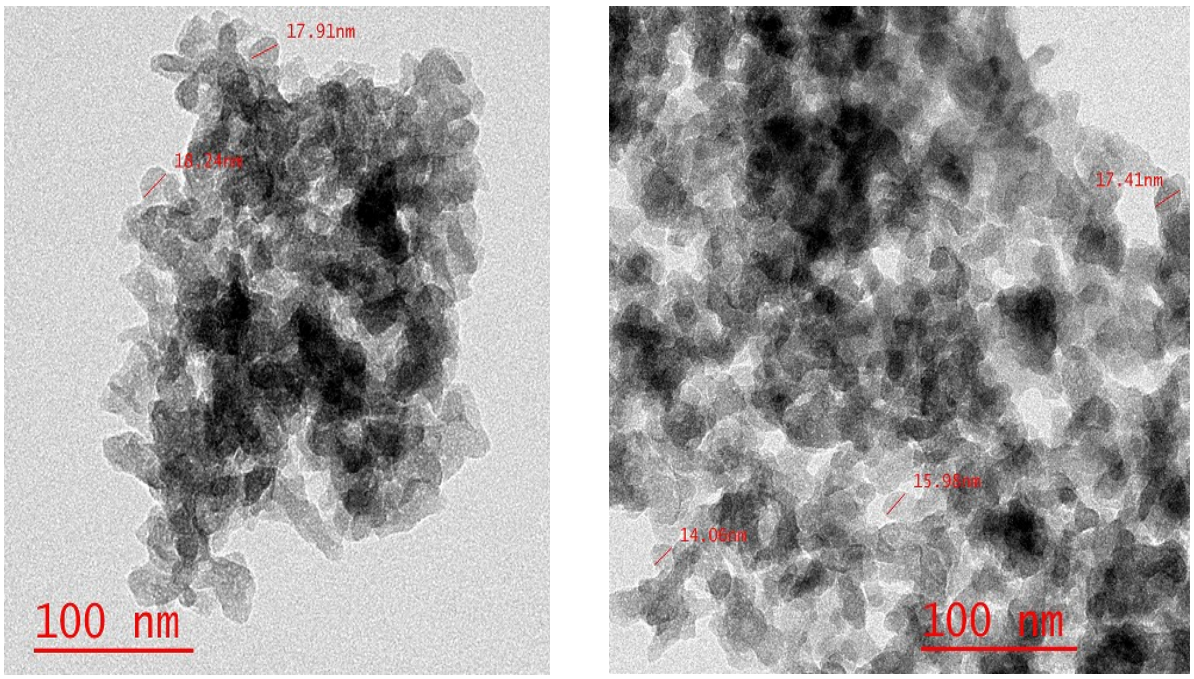

Figure 3-13: TEM images of superhydrophobic SiO_2 nanoparticles.

3.4.7 Membrane performance

The effect of changing nanoparticles concentration on the pure water flux of the composite membranes is shown in Fig. 3-14. From the results, it is evident that the flux increases upon addition of nanoparticles from MS-0 to MS-4 and as the nanoparticles concentration further

increases, shows a maximum at the nanoparticle concentration of 7 wt. % (MS-7). This trend parallels to the pore size change in Fig. 3-7, which also shows a maximum at 7 wt. % due to the agglomeration of nanoparticles at higher concentrations. The decrease in porosity with an increase in nanoparticles concentration (see Fig. 3-6) also contributes to the flux decrease at concentrations higher than 7 wt. %. It is also likely that some of the pores formed at the high nanoparticle concentration were dead-end pores through which no flow occurred [25].

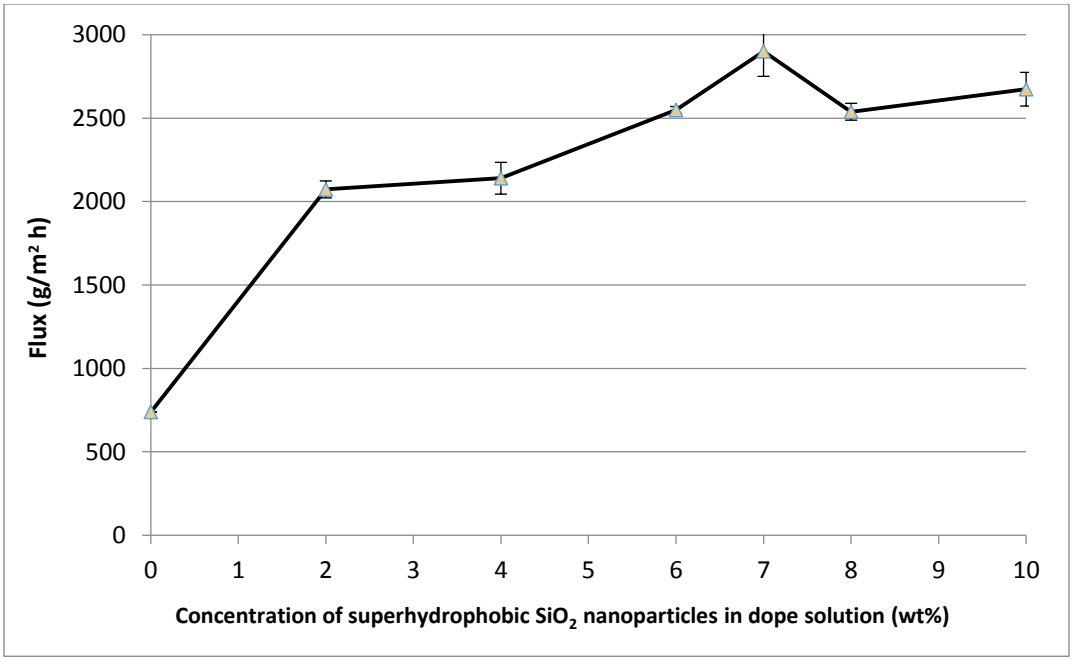

Figure 3-14. Permeation flux of VMD as a function of nanoparticles concentration in dope solution.

The nanocomposite membranes where further tested for salt rejection with a 35 g/L NaCl solution to mimic sea water and 2 g/L NaCl brackish water as the feed at 27°C. The conductivity of the salt water feed (510 mS/m) yielded a permeate solution (< 70 μS/m) denoting a salt rejection > 99.98% at the maximum flux of 2.9 kg m^{-2} h^{-1} while the brackish water (3.94 mS/m) yielded a permeate of < 50 μS/m giving a 99.99% rejection (Fig. 3-15) for the MS-7

nanocomposite membrane which contained 7 wt. % superhydrophobic nanoparticles. This flux corresponds to 4 times higher than the VMD flux of the neat membrane, implying incorporating nanoparticles of up 7 wt. % in the dope solution is optimal under the investigated conditions.

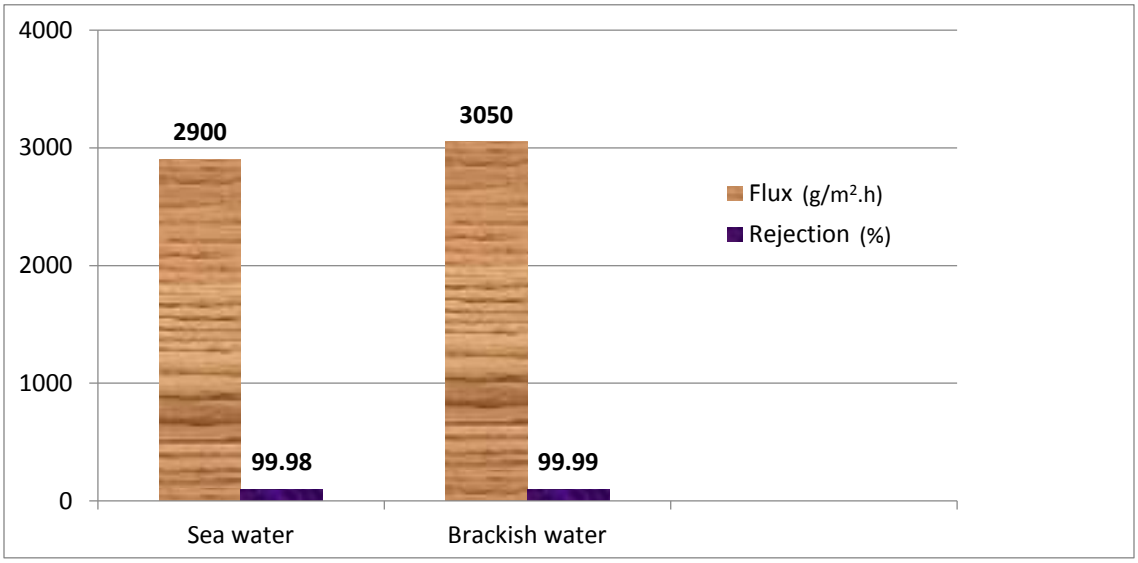

Figure 3-15: Analysis of membrane flux with artificial seawater, i.e., containing 35 g/L NaCl and artificial brackish water, i.e., 2 g/L aqueous NaCl solution.

Usually, greater flux is associated with higher porosity [12], which was not the case in this study. Despite having the highest porosity, the neat PVDF membrane showed the lowest flux, implying vapour flux does not depend solely on the porosity but also on the resistance to the vapour movement across the membrane (dense crystalline nature) [7]. The MS-7 nanocomposite flux was analysed with respect to time to study the flux and rejection stabilities. Fig. 3-16 shows an initial drop in flux of about 0.5% and then the flux levels off to 2991 g/m^2 h. The same trend of very small decrease of performance in the first four hours also applies to the rejection. It can thus be deduced that, for the time duration specified, the flux and rejection of the fabricated membrane were stable.

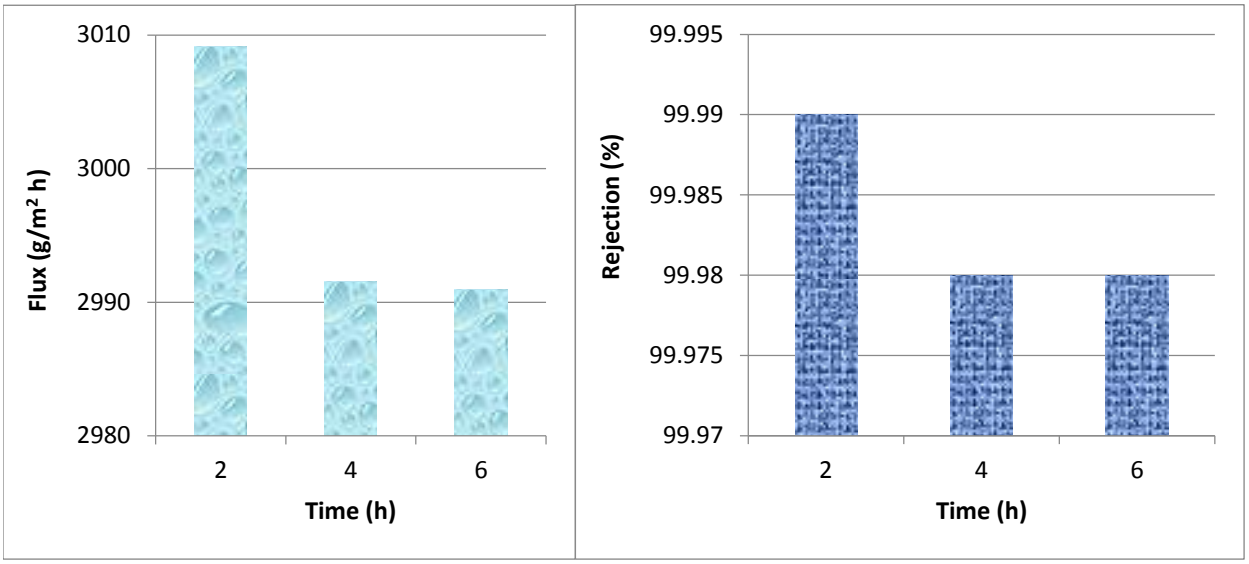

Figure 3-16. Comparative analysis of flux stability and rejection with time

A comparative analysis of the sponge-like layer thickness in relation to the vapour flux showed that, as the sponge-like layer thickness decreased, the flux increased with the MS-7, showing the thinnest sponge-like layer and greatest flux. As the concentration of the nanoparticle increased further, the sponge-like layer thickness started to increase hence flux takes a downward turn.

When compared to the neat PVDF, all the nanocomposite membranes showed a greater flux, implying the less resistance presented by the thinner sponge-like layer couple with the increased pore size. In other words, our results indicated that the sponge-like layer of membrane contributed greatly to the resistance of mass transfer of vapour, which may result in a difference of VMD flux of up to 4 folds or more.

3.5 Conclusions

In summary, flat sheet nanocomposite PVDF-SiO_2 membranes were prepared by the phase inversion technique, characterized by various methods and their performance in VMD was

investigated. The experimental results showed that the addition of superhydrophobic SiO_2 nanoparticles have varying effects. The nanocomposite membrane morphology showed an asymmetric structure with a finger-like macro-void layer and a sponge-like layer, the ratio of which had an impact on the VMD performance of the membrane. The maximum flux was observed at the nanoparticle concentration of 7 wt. % with an average flux of around 3 kg/m^2 h, which was 4 times higher than the neat PVDF membrane. A salt rejection of more than 99.98% indicates that the fabricated membrane is satisfactory for membrane distillation. The results denote that 7 wt. % is the concentration most suitable for the studied VMD conditions. It was observed that the porosity decreased while the flux increased with increase in nanoparticles concentration. It is thus evident that the VMD flux does not depend solely on the porosity of the membrane but also on the crystalline nature of the membrane. On the other hand, all nanocomposite membranes showed an increased pore size compared to the neat PVDF membranes thus pore size also accounted for the increased flux. It is hence likely that the flux is determined by the interplay of surface pores size and bulk porosity. Also, all nanocomposite membranes had LEP_w values > 3 bar making them suitable for VMD applications. The study concludes that PVDF blended with superhydrophobic SiO_2 nanoparticles is suitable for VMD processes for desalination of sea water.

3.6 Acknowledgments

Special thanks to Arkema Inc. (Philadelphia, PA) for their generously offer of the polymers (Kynar® 740 and Kynar® HSV 900). Financial supports of the NSERC Discovery (Grant # RGPIN 288226-2010) and the I2IPJ (Grant # 463142-2014) grants are also gratefully acknowledged.

3.7 References

[1] (a) Anonymous, The United Nations Document Index, The United Nations Publications, New York, NY, 2005, 22.03.2005, Retrieved May 12, 2015; (b) Anonymous, International Decade for Action "Water for Life" 2005-2015, The UN-Water Decade Programme on Advocacy and Communication (UNW-DPAC), doi: ///www.un.or/waterforlifedecade/, Retrieved May 12, 2015; (c) Anonymous, Managing Water Under Uncertainty and Risk, The United Nations World Water Development Repot (WWDR4), 4th Edition, UNESCO, Paris, France, 2012, ISBN: 978-92-3-104235-5; (d) Anonymous, Water in a Sustainable World, The United Nations World Water Development Repot 2015, UNESCO, Paris, France, 2015, ISBN: 978-92-3-100071-3

[2] Abu-Zeid, M. A. E., Zhang, Y., Dong, H., Zhang, L., Chen, H., & Hou, L. (2015). A comprehensive review of vacuum membrane distillation technique. *Desalination, 356*, 1–14.

[3] Bian, X., Shi, L., Yang, X., & Lu, X. (2011). Effect of nano-TiO_2 particles on the performance of PVDF, PVDF-g-(maleic anhydride), and PVDF-g-poly(acryl amide) membranes. *Industrial & Engineering Chemistry Research, 50*(21), 12113–12123.

[4] Bonyadi, S., & Chung, T. S. (2007). Flux enhancement in membrane distillation by fabrication of dual layer hydrophilic-hydrophobic hollow fibre membranes. *Journal of Membrane Science, 306*(1-2), 134–146.

[5] Chen, Z., Rana, D., Matsuura, T., Yang, Y., & Lan, C. Q. (2014). Study on the structure and vacuum membrane distillation performance of PVDF composite membranes: I. Influence of blending. *Separation and Purification Technology, 133*, 303–312.

[6] Chen, Z., Rana, D., Matsuura, T., Meng, D., & Lan, C. Q. (2015). Study on the structure and vacuum membrane distillation performance of PVDF membranes: I. Influence of molecular weight. *Chemical Engineering Journal, 276*, 174–184.

[7] Chiam, C., & Sarbatly, R. (2013). Vacuum membrane distillation processes for aqueous solution treatment - A review. *Chemical Engineering and Processing: Process Intensification, 74*, 27–54.

[8] Cui, A., Liu, Z., Xiao, C., & Zhang, Y. (2010). Effect of micro-sized SiO_2-particle on the performance of PVDF blend membranes via TIPS. *Journal of Membrane Science, 360*(1-2), 259–264.

[9] Dong, Z., Ma, X., Xu, Z., You, W., & Li, F. (2014). Superhydrophobic PVDF–PTFE electrospun nanofibrous membranes for desalination by vacuum membrane distillation. *Desalination, 347*, 175–183.

[1] Drioli, E., Ali, A., & Macedonio, F. (2015). Membrane distillation: Recent developments and perspectives. *Desalination, 356*, 56–84.

[2] Fan, H., & Peng, Y. (2012). Application of PVDF membranes in desalination and comparison of the VMD and DCMD processes. *Chemical Engineering Science, 79*, 94–102.

[3] Fontananova, E., Jansen, J. C., Cristiano, A., Curcio, E., & Drioli, E. (2006). Effect of additives in the casting solution on the formation of PVDF membranes. *Desalination, 192*(1-3), 190–197.

[4] Hou, D., Dai, G., Fan, H., Wang, J., Zhao, C., & Huang, H. (2014). Effects of calcium carbonate nano-particles on the properties of PVDF/nonwoven fabric flat-sheet composite membranes for direct contact membrane distillation. *Desalination, 347*, 25–33.

[5] Khayet, M., & Matsuura, T. (2011). *Membrane Distillation*: *Principles and Applications*, Ch. 12, pp. 323–359, Elsevier, Amsterdam, The Netherlands.

[6] Koo, J., Han, J., Sohn, J., Lee, S., & Hwang, T. (2013). Experimental comparison of direct contact membrane distillation (DCMD) with vacuum membrane distillation (VMD). *Desalination and Water Treatment, 51*(31-33), 6299–6309.

[7] Kuo, C., Lin, H., Tsai, H., Wang, D., & Lai, J. (2008). Fabrication of a high hydrophobic PVDF membrane via nonsolvent induced phase separation. *Desalination, 233*(1-3), 40–47.

[8] Li, G., Shen, L., Luo, Y., & Zhang, S. (2014). The effect of silver-PAMAM dendrimer nanocomposites on the performance of PVDF membranes. *Desalination, 338*, 115–120.

[9] Li, X., Zhang, M., He, J., Wu, D., Meng, J., & Ni, P. (2014). Effects of fluorinated SiO2 nanoparticles on the thermal and electrochemical properties of PP nonwoven/PVdF-HFP composite separator for li-ion batteries. *Journal of Membrane Science, 455*, 368–374.

[10] Naidu, G., Jeong, S., Choi, Y., Jang, E., Hwang, T., & Vigneswaran, S. (2014). Application of vacuum membrane distillation for small scale drinking water production. *Desalination, 354*, 53–61.

[11] Ortiz de Zárate, J. M., Peňa, L., & Mengual, J. I. (1995). Characterization of membrane distillation membranes prepared by phase inversion. *Desalination, 100*(1-3), 139–148.

[12] Peng, P., Fane, A. G., & Li, X. (2005). Desalination by membrane distillation adopting a hydrophilic membrane. *Desalination, 173*(1), 45–54.

[13] Pourjafar, S., Jahanshahi, M., & Rahimpour, A. (2013). Optimization of TiO2 modified poly(vinyl alcohol) thin film composite nanofiltration membranes using taguchi method. *Desalination, 315*, 107–114.

[14] Qtaishat, M., Khayet, M., & Matsuura, T. (2009). Novel porous composite hydrophobic/hydrophilic polysulfone membranes for desalination by direct contact membrane distillation. *Journal of Membrane Science, 341*(1-2), 139–148.

[15] Razmjou, A., Arifin, E., Dong, G., Mansouri, J., & Chen, V. (2012). Superhydrophobic modification of TiO_2 nanocomposite PVDF membranes for applications in membrane distillation. *Journal of Membrane Science, 415-416*, 850–863.

[16] Salimi, A., & Yousefi, A. A. (2003). Analysis method: FTIR studies of β-phase crystal formation in stretched PVDF films. *Polymer Testing, 22*(6), 699–704.

[17] Devi, S., Ray, P., Singh, K., & Singh, P. S. (2014). Preparation and characterization of highly micro-porous PVDF membranes for desalination of saline water through vacuum membrane distillation. *Desalination, 346*, 9–18.

[18] Teoh, M. M., & Chung, T. (2009). Membrane distillation with hydrophobic macrovoid-free PVDF–PTFE hollow fibre membranes. *Separation and Purification Technology, 66*(2), 229–236.

[19] Tijing, L. D., Choi, J., Lee, S., Kim, S., & Shon, H. K. (2014). Recent progress of membrane distillation using electrospun nanofibrous membrane. *Journal of Membrane Science, 453*, 435–462.

[20] Wang, P., & Chung, T. (2015). Recent advances in membrane distillation processes: Membrane development, configuration design and application exploring. *Journal of Membrane Science, 474*, 39–56.

[21] Wang, X., Zhang, L., Sun, D., An, Q., & Chen, H. (2009). Formation mechanism and crystallization of poly(vinylidene fluoride) membrane via immersion precipitation method. *Desalination, 236*(1-3), 170–178.

[22] Winter, D., Koschikowski, J., & Wieghaus, M. (2011). Desalination using membrane distillation: Experimental studies on full scale spiral wound modules. *Journal of Membrane Science, 375*(1-2), 104–112.

[23] Yang, Y., Rana, D., Matsuura, T., Zheng, S., & Lan, C. Q. (2014). Criteria for the selection of a support material to fabricate coated membranes for a life support device. *RSC Advances*, *4*(73), 38711–38717.

[24] Baghbanzadeh, M., Rana, D., Matsuura, T., & Lan, C. Q. (2015). Effects of hydrophilic CuO nanoparticles on properties and performance of PVDF VMD membranes. *Desalination*, *369*, 75–84.

4 Performance enhancement of PVDF/Superhydrophobic SiO_2 nano-composite membrane by electro-spun dual layer for vacuum and direct contact membrane distillation

Abstract

Membrane distillation (MD) is a promising separation technique capable of being used in desalination of marine and brackish water. PVDF flat sheet nano-composite membranes were surface modified by coating with electro-spun PVDF nano-fibres to increase the surface hydrophobicity. For this purpose, the nano-composite membrane containing 7 wt. % superhydrophobic SiO_2 nano-particles, which showed the highest flux in our previous work, was then first subjected to pore size augmentation by increasing the concentration of the pore forming agent (Di-ionized water). Then, the flat sheet membranes so prepared were subjected to the nanofibre coating by electro-spinning. The uncoated and coated composite membranes fabricated were characterized using contact angle, liquid entry pressure of water, and scanning electron microscopy. The membranes were further tested for 6 h desalination by direct contact membrane distillation (DCMD) and vacuum membrane distillation (VMD), with a 3.5 wt. % synthetic $NaCl_{aq}$ as the feed at 27.5 ^{o}C and cold side maintained at 15±2 ^{o}C. For VMD, vacuum of 94.8 kPa was applied. The maximum permeate flux achieved was 3.2 kg/m^2.h for VMD and 6.5 kg/m^2.h for DCMD. The salt rejection obtained was higher than 99.98%. The coated membranes showed a more stable flux than uncoated membrane indicating that double layered membranes have great potential in solving the pore wetting problem in MD.

Keywords: Polyvinylidene fluoride, superhydrophobic SiO_2 nanoparticles, PVDF nano-fibres, vacuum membrane distillation, direct contact membrane distillation.

4.1 Introduction

Reverse osmosis (RO) is still considered today as the world's leading process in desalination of seawater and brackish water even though membrane distillation (MD) has been showing greater potentials in the last decade[1]. MD is a thermally driven process involving a micro porous, semi permeable, hydrophobic membrane through which only water vapour can diffuse. With the four main configurations of MD established; direct contact membrane distillation (DCMD), vacuum membrane distillation (VMD), air gap membrane distillation (AGMD) and sweep gas membrane distillation (SGMD), the improvement of MD process has been going on with a special focus on the development of a suitable and effective membrane for the process. Some of the key advantages in using MD for desalination over RO are the high purity of the permeate, no extensive feed pre-treatment involved, relatively high product water recoveries, and the energy consumption that could be minimal in so far as the heat is obtained from a waste source[2].

When it comes to large scale desalination operations, MD is lagging behind RO because most of the membranes that have been developed for the process are more or less reliable only for very short time intervals, the trans-membrane flux achieved so far seem not to be stable over time and the durability of membrane is still under investigation. Irrespective of the MD configuration in operation, the MD membrane has to be hydrophobic with a reasonable liquid entry pressure (LEP_w) to prevent pore wetting. The pore size should not be so small to prevent vapour molecules from passing through and so large as to allow feed liquid to pass through[3]. Pore wetting is a consequence of feed liquid penetrating through the membrane pores hence decreasing the membrane rejection capabilities alongside compromising the separation process. It is for this reason that researchers are paying keen attention to the development of MD membranes with high hydrophobicity, reasonable LEP_w, and capability of high and stable flux including enhanced durability (mechanical stability). Since the LEP_w is directly related to the

pore size of the membrane; the larger the pore size the lower the LEP_w and vice versa, researchers have used different pore forming agents to optimize the LEP_w to prevent pore wetting. According to the recommendation made by Drioli and Schneider[4], for a reasonable LEP_w to be attained, the pore radius should range between 0.5-0.6 μm. Hydrophobic flat sheet membranes were fabricated by Tomaszewska[5] using LiCl as pore forming agent and the effect on the flux was studied. Khayet and Matsuura[6] used pure water as pore forming additives for the fabrication of supported and unsupported PVDF membranes.

Different polymers have also been used to fabricate hydrophobic membranes due to the low surface energies of the polymers. PVDF, PTFE, and PP are the most common polymers used for MD membranes. Kuo et al [7] prepared superhydrophobic PVDF membranes by using alcohol as the coagulation bath and tested for desalination. Shirazi et al [8] also prepared hydrophobic PTFE membranes for characterization by atomic force microscopy.

Nanomaterials and inorganic materials [9] have been incorporated into membrane dope solutions to enhance the membrane hydrophobicity and performance. Zirconium dioxide (ZrO_2)[10], aluminium oxide (Al_2O_3)[11] and titanium dioxide (TiO_2)[12] have been blended with PVDF polymer to produce membranes with improved performances, thermal properties and mechanical stability. Also, backing materials have been used as support in membrane fabrication to increase mechanical stability and performance of MD membranes. Yang et al[13] produced PVDF membranes on support material and saw a 15 fold increase in flux when compared to the unsupported membrane.

Recently, the technique of electro-spinning has been exploited to produce nano-fibres for use as MD membranes. These electro-spun nano-fibres turn to produce highly hydrophobic surfaces due to increased surface roughness[14] with high porosity (potentials of good MD

membranes). Though these nano-fibres mats have relatively lower LEP_w with an increased chance of pore wetting due to larger pore sizes, they have been used to modify the surfaces of flat sheet membranes[15] by forming, dual and triple layer MD membranes. Prince et al[16] produced an innovative design to help prevent pore wetting by using nano-fibres based hydrophilic/hydrophobic membrane with a thin hydrophobic nano-fibres layer on the top and a thin hydrophilic nano-fibres layer on the bottom of the conventional casted micro-porous layer.

In our previous work, the effect of the concentration of superhydrophobic SiO_2 nano-particles in the casting dope was studied when flat-sheet PVDF membranes were prepared by the conventional phase inversion method and their performance tested by VMD.

The objective of this work is to further improve the performance of the membrane that has best performed in the VMD desalination process in our previous work.

To achieve this goal, the task of this work consist of the following two steps; i.e. 1) the effect of adding water as pore former to the above prepared SiO_2 blended PVDF membrane on the pore size, pore size distribution will be studied and the MD flux will be investigated. 2) The effect of coating the surface of the membrane prepared in step 1) with a thin layer of electro-spun nanofibre layer on the VMD and DCMD performance is investigated. A 3.5 wt. % NaCl aqueous solution is used as the feed for MD desalination.

4.2 Experimental

4.2.1 Materials

Poly(vinylidene fluoride) (PVDF) polymer of two different molecular weights: Kynar® 740 and Kynar® HSV 900 was supplied as resins and powder respectively from Arkema Inc., Philadelphia, PA. Dimethyl acetamide (DMAc, > 99%) used as solvent was supplied by Sigma

Aldrich Inc., St. Louis, MO. Deionised water (conductivity < 10 μS/m) produced by Millipore Q BIOCEL unit, Millipore, Billerica, MA, was used as the pore forming agent as well as coagulation agent. Superhydrophobic silica nanoparticles (purity: ≥ 99.8%, particle size: 10-20 nm, surface area: 100-140 m^2/g), surface modified with single layer organic chains were supplied by SkySpring Nanomaterials Inc. (Houston, TX), Acetone (> 99.99%) was purchased from Sigma Aldrich Inc., St. Louis, MO.

4.2.2 Membrane preparation

4.2.2.1 Preparation of membrane by phase inversion

Flat sheet membranes were prepared using PVDF as base polymer, DMAc as base solvent and DI water as non-solvent (pore former) additive. The composition of the dope solution is shown in table 4-1. To prepare the dope solution two kinds of PVDF, DMAc, and water were first mixed under vigorous stirring at 180 rpm and 50^oC for 72 h to ensure complete dissolution of the polymer. The solution was then allowed to de-gas for at least 24 h at room temperature. 7 wt. % SiO_2 nano-particles were then added to the required quantity of the polymeric solution and stirred at 100 rpm for 2 h. The dope solution so prepared was cast onto a glass plate at room temperature using a 250 μm thickness casting bar. After casting, the dope film was kept staying on the glass plate for 20 s followed by complete immersion into the water bath at room temperature for coagulation. Upon contact with the water, polymer coagulation took place producing a white flat sheet membrane. The membrane was then left in the water bath for 24 h period to remove residual solvent, and then dried at room temperature prior to nanofibre coating and membrane characterization. The membranes prepared from the dope M1, M2, and M3 (see table 4-1) were also coded as M1, M2 and M3.

Table 4-1. Dope solution composition for phase inversion membranes.

	Composition of polymeric solution before adding SiO_2 nanoparticles			
	PVDF			
Sample ID	**Kynar®740 (wt. %)**	**Kynar®HSV 900 (wt. %)**	**Water (wt. %)**	**DMAc (wt. %)**
M1	9	6	1.25	83.75
M2	9	6	1.875	83.125
M3	9	6	2.5	82.5

*To prepare the dope solution 7 wt. % of SiO_2 nano-particles were added to 93 wt. % of the polymeric solution

4.2.2.2 Preparation of membrane by electrospinning

PVDF electro-spinning solution containing 15 wt. % PVDF and 2:3 ratio (w:w) of DMAc to acetone was prepared. The solution composition is given in Table 4-2. The polymer solution was stirred at 50^{o}C for 24 h and another 24 h for cooling at room temperature. Electro-spinning was carried out using the equipment shown in Fig. 4-1. Twenty mL of the polymer solution was electro-spun on all M1-M3 membranes at a spinning rate of 1 mL/h, with a voltage of 15 kV applied between the spinneret and rotating drum placed 150 mm apart from each other. The flat sheet nano-composite membrane now coated with nano-fibres was then allowed to dry at room temperature for solvent to evaporate before further characterization. The coated membranes were coded as M1C, M2C and M3C membrane respectively.

Table 4-2. Electro-spinning solution composition.

PVDF **Kynar®740 (wt. %)**	DMAc (wt. %)	Acetone (wt. %)
15	34	51

4.3 Membrane characterization

4.3.1 Water contact angle

The water contact angle (CAw) of the nano-composite membrane and the nano-fibres coated membranes was measured using a VCA Optima Surface Analysis System (AST Products Inc., Billerica, MA). The samples were cut into tiny strips and edges affixed unto a slide using a translucent tape. With the aid of a micro syringe (Hamilton Company, Reno, NV), 1 μL of DI water droplet was placed on the membrane surface and the contact angle was measured after a 10 s wait period. Measurements were taken from 5 randomly selected spots and the average was reported.

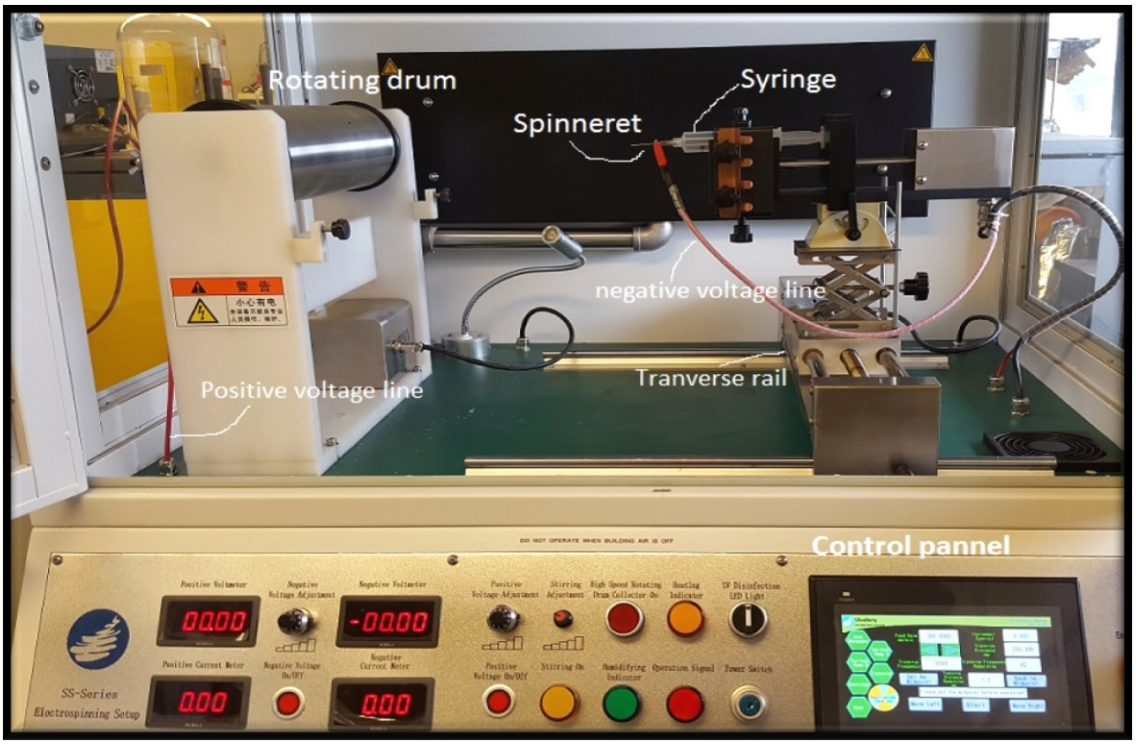

Figure 4-1. Electro-spinning equipment

4.3.2 Liquid entry pressure

The liquid entry pressure of water (LEP_w) of the coated and uncoated membranes was measured. The schematic of the LEP_w measurement setup was is shown in our previous work. The static liquid chamber carrying the membrane sample (area, 0.131 m^2) was filled with 200 mL of DI water at ambient temperature and the pressure was to the liquid from a nitrogen cylinder at a constant rate of 2 psi per 10 min with the aid of a control valve, until the water starts dropping off from the outlet. The pressure was noted and the process repeated thrice with different membrane samples at the same conditions and the average value noted.

4.3.3 Scanning electron microscopy

The surface of both uncoated (M1-M3) and the coated (M1C-M3C) membrane was observed by Scanning Electron Microscope (SEM), Tescan, Vega-II XMU with Oxford Inca Energy 250X EDS. The cross-section of the M1-M3 membranes were also observed by SEM. Liquid nitrogen was used to break the membranes in order to have shape edges for easy viewing. The embrittled samples were then coated with gold (> 99.8%) under vacuum using an Anatech Hummer VII to increase sample conductivity. SEM observations were then made at random positions using a suitable magnification to evaluate the effect of water concentration and nano-fibres coating.

4.3.4 Pore size and pore size distribution

The surface pore sizes were determined by the analysis of the top surface SEM images using the ImageJ software. Approximately 100 pores, randomly selected were analysed and the results shown as an average.

4.3.5 Surface roughness

The top surface of M1 and coated M1 membrane was analysed for roughness. The software ImageJ was used for the analysis where SEM images were converted to 32 bits images and with the aid of an inbuilt plugin of ImageJ (*SurfCharJ*), the roughness could be computed on image size of 7.5 μm x 7.5 μm to determine the average roughness (R_a) of the analysed area.

4.3.6 Membrane performance by DCMD

Both uncoated and coated membranes were subjected to DCMD experiment using a setup (continuous) described schematically in Fig. 4-1. The performances of both membranes were compared with respect to the flux and salt rejection using a membrane with an effective area of 0.385 m^2. The feed tank was filled with saline water and pumped to the feed side of the

permeation cell using a circulation pump at a flow rate of 2 L/m. Chilled water on the permeate side of the permeation cell was supplied from a cooling tank and pumped at a flow rate of 2 L/m.

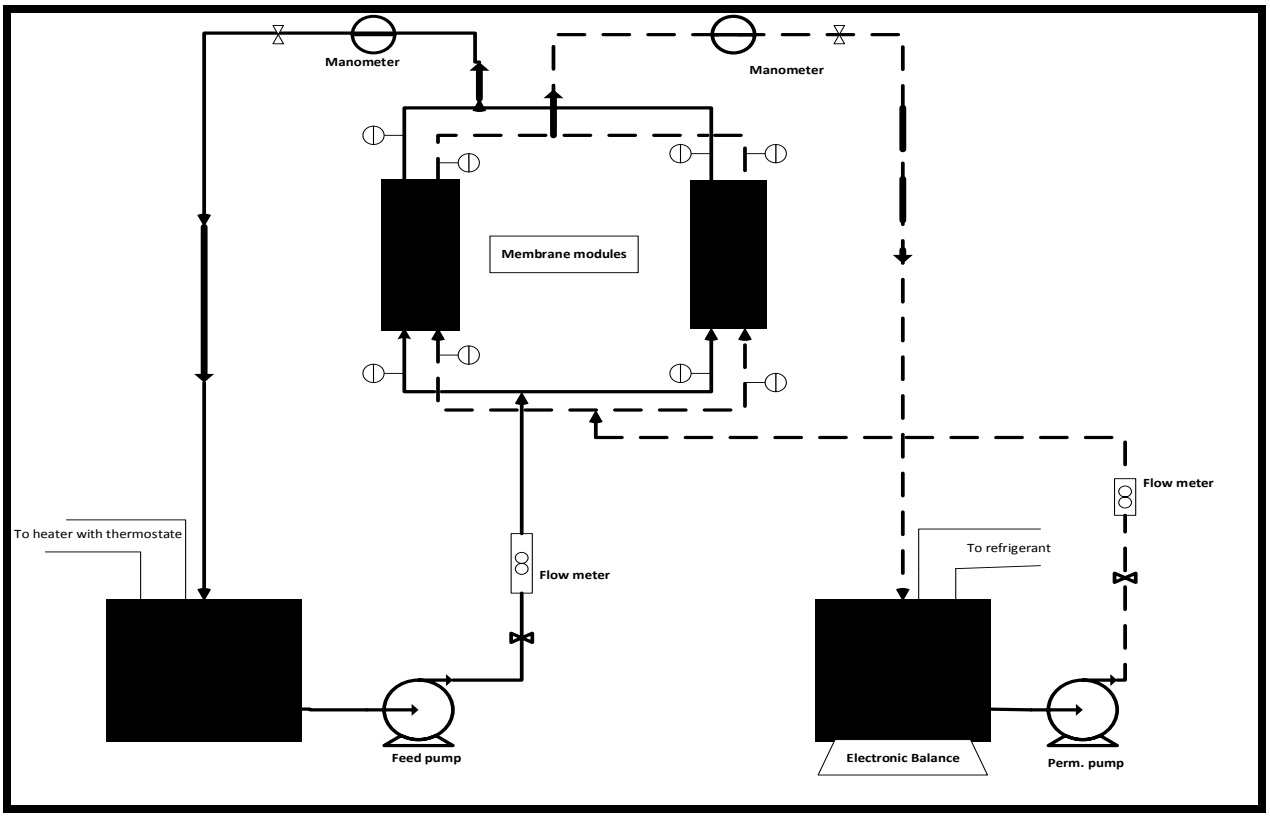

Figure 4-2. Schematic of the DCMD setup.

The temperatures were measured by the thermometers installed at the inlets and outlets of the cells. Pressure gauges were also used to monitor the pressure on the feed and permeate side of the permeation cell to avoid any pressure difference between both sides. The permeate flux was measured by monitoring the water level in both tanks. Assuming that no water losses or leakages occur, a reduction in weight on the feed side, should correspond exactly to the increase in the permeate side. This gain on the permeate side, is shown as an increase in weight on the electronic scale balance. The DCMD experiment was carried out using synthetic seawater (3.5 wt. % $NaCl_{aq}$) heated and kept at 27.5 ^{o}C by a thermostatic controlled heater. The chilled water was kept at a temperature of 15 ± 2 ^{o}C for all membranes tested and for all runs.

4.3.7 Membrane performance by VMD

All the membranes fabricated both uncoated and nano-fibre coated, were tested for VMD. The setup used for VMD was shown in our previous work [17-18]. The permeation cell (static) consisted of a feed chamber with a permeation base where the membrane (area, 0.113 m^2) was placed. A vacuum pump was used to apply vacuum (94.8 kPa) on the permeate side so that the permeated water vapour could be collected. The feed chamber was maintained at 27°C with the use of a heating coil connected to a temperature controlled bath and kept under agitation to minimise temperature polarization effects. The procedure involved a 1 h pre-treatment by which air and moisture were sucked out of the lines. By doing so, the system was allowed to reach a steady state. All cold traps were cooled using liquid nitrogen. After the vapour from the lines was collected in one cold trap during the 1 h pre-treatment, the vacuum line was switched to the other cold trap where the permeate vapour was collected to measure the flux. The experiment was conducted for a predetermined time and the flux calculated using equation 1.

$$\text{Flux} = \frac{w}{t.A} \tag{1}$$

Where w (g) is the weight of condensate, t (h) is the time of flux collection, A (m^2) is the effective membrane surface area.

4.4 Results

4.4.1 Membrane characterization

SEM image analysis

The top surface SEM images of all the uncoated membranes as well as the electro-spun nanofibre mat are shown in Fig. 4-3. As for the uncoated membranes, a large number of pores are observed at the top surface with a gradual increase in pore size from 140 ± 20nm of M1 to 175 ± 15nm of M3, which is ascribed to the intrusion of a larger quantity of water from the coagulant bath induced by the presence of the larger quantity of water in the casting dope.

Water being the nonsolvent media and the SiO_2 nanoparticles are superhydrophobic implying the rate of demixing of these two is slow resulting in much larger pores[19]. Also the number of pores of M2 and M3 was considerably more than M1

The cross sectional images (Fig. 4-4) shows a typical asymmetric morphology with a finger-like macro-void layer and a sponge-like layer. Compared to M1 membrane, the size of the finger-like macro-void of M2 and M3 was slightly larger (in depth and breadth), which could be noticed on the slight but minimal change in distillation flux.

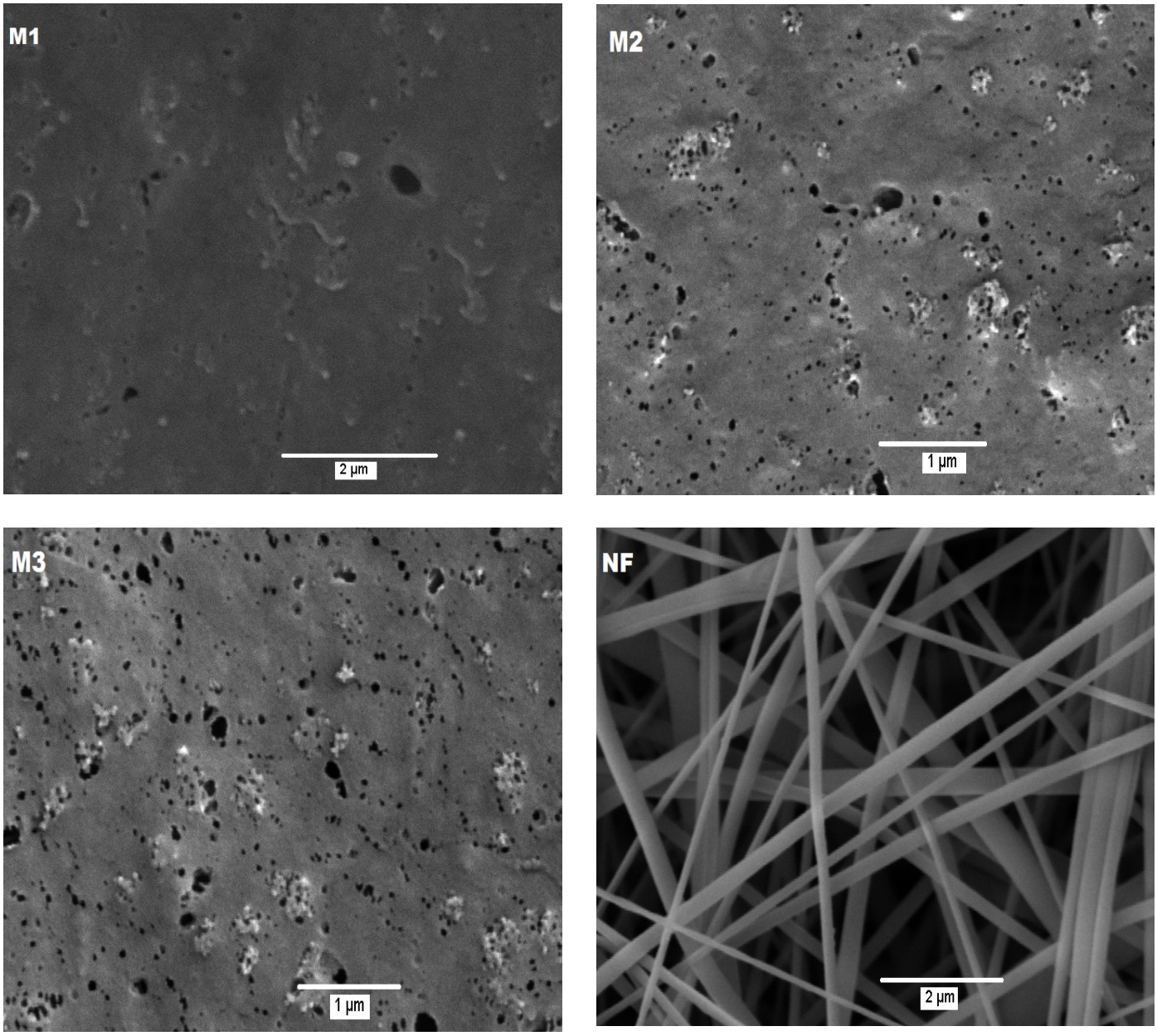

Figure 4-3. Top surface SEM images of flat sheets (M1-M3) and nano-fibres (NF)

A closer look at the sponge layer (Fig. 4-5) reveals that the sponge-like layer of M3 is denser than M1

The SEM image of the PVDF nano-fibres, electro-spun without any substrate is also shown in Fig. 4-3. From the images, the average fibre diameter of the nano-fibres ranges from 80

to 220 nm with an average pore size 1.32±0.33 μm. Since the nano-fibres will be electro-spun on top of the substrate membrane, the size of the surface pores should be representative of the nano-fibre layer. As well, since only a very thin layer of the nano-fibres was coated on the substrate membrane (25 μm), and the porosity of the nano-fibres mats is relatively high [20], it implies that the trans-membrane flux experiences only little transport resistance as a result of the coating but the surface of the coated membrane experiences increased hydrophobicity due to the presence of the nano-fibres layer.

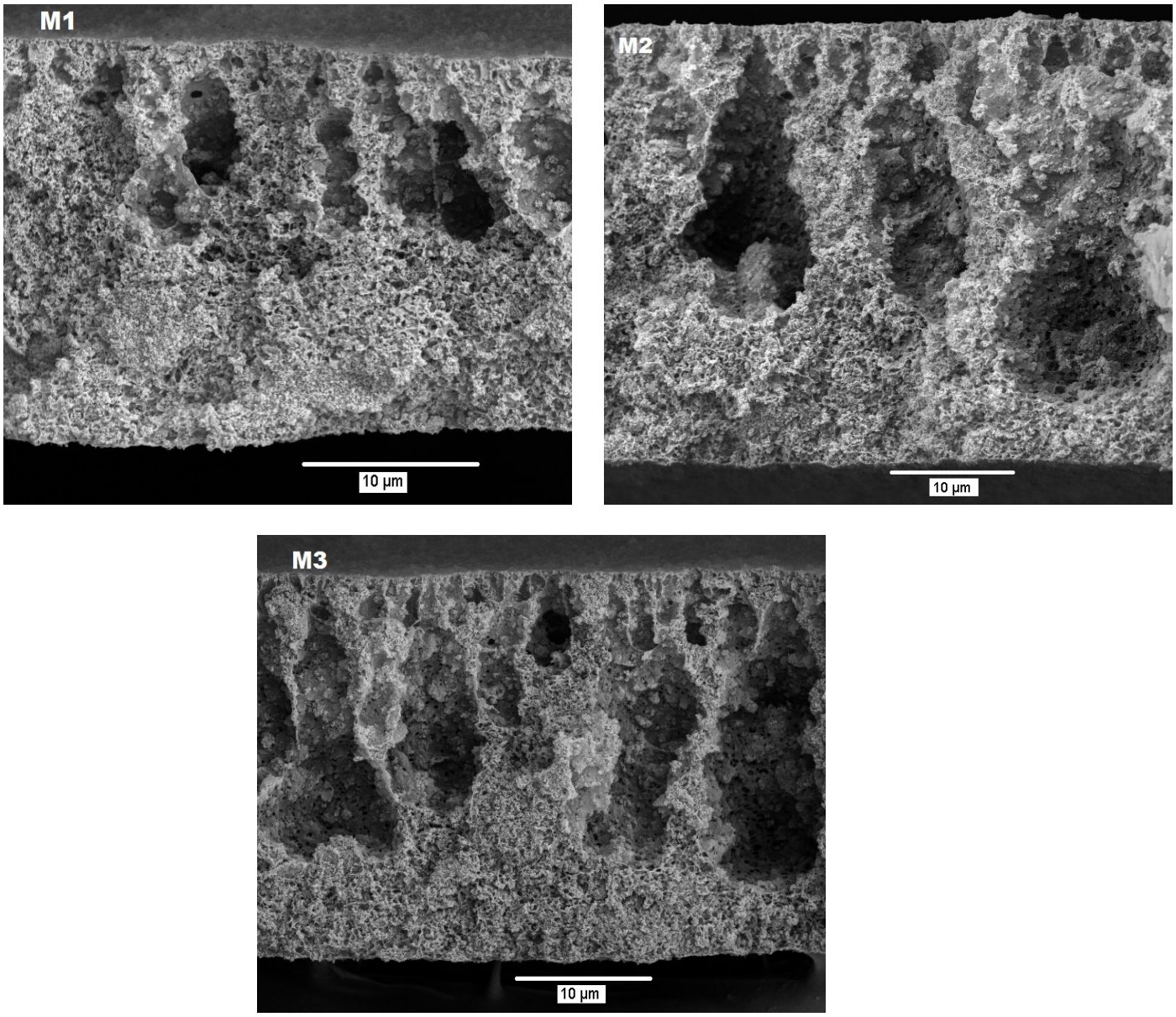

Figure 4-4. Cross sectional images of fabricated flat sheet membranes.

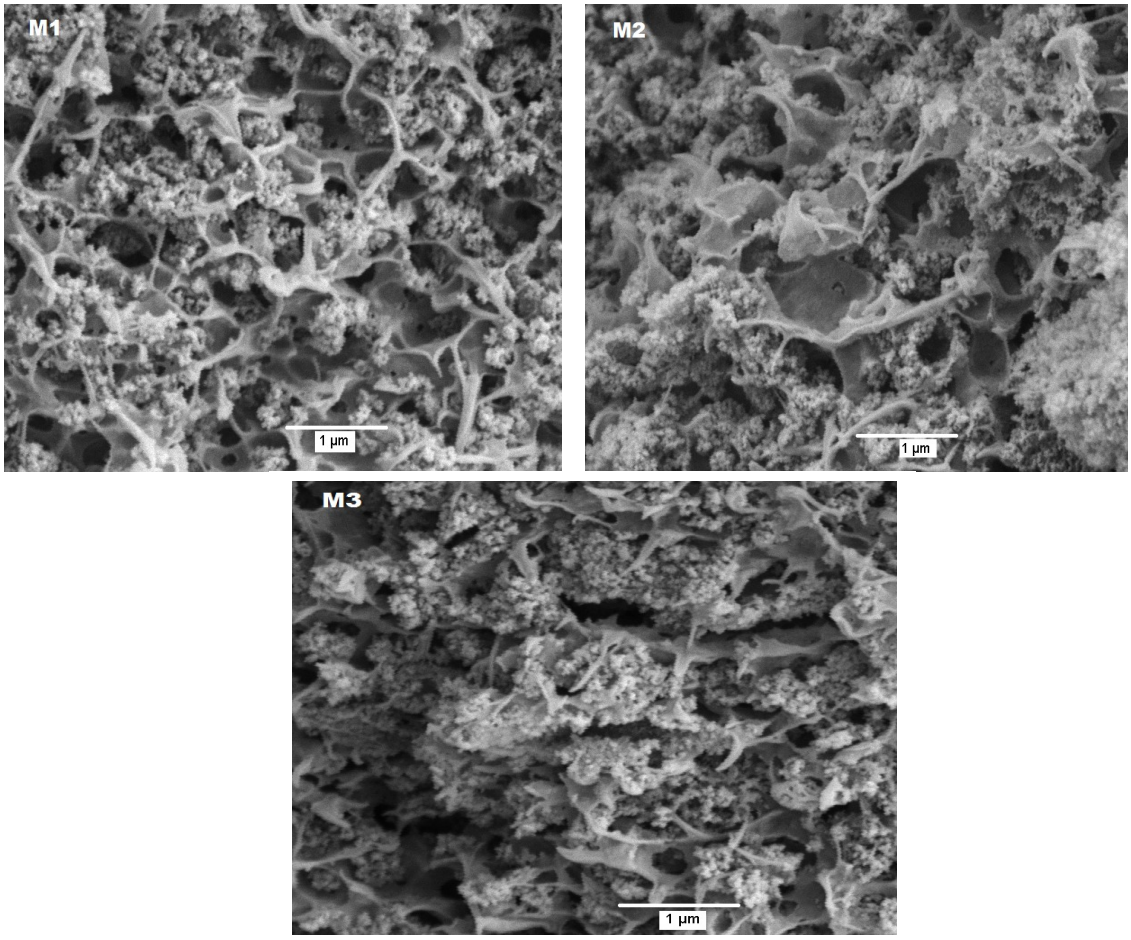

Figure 4-5. Sponge- like layer analysis of the flat sheet membranes.

The LEP_w analysis of the membranes is shown on Fig. 4-6. From the figure, LEP_w decreases from 448 kPa of M1 to 241 kPa of M3 as the water content in the casting dope increased. This reduction ties with the increase in pore size, since pore size is inversely proportional LEP_w. It therefore follows that, doubling the water content of the dope solution resulted in 86% reduction in LEP_w. Upon coating the surface with thin layer of nano-fibres, a significant increase in LEP_w is seen, i.e. a 26% increase from M1 to M1C and a 57% increase from M3 to M3C. Since the coated surface was hydrophobic, it helped prevent liquid from penetrating the pores hence increasing the LEP_w. The nano-fibres mat alone showed a relatively

low LEP_w value of < 96.5 kPa but when nano-fibres were electro-spun directly on the substrate membranes, the LEP_w increased drastically.

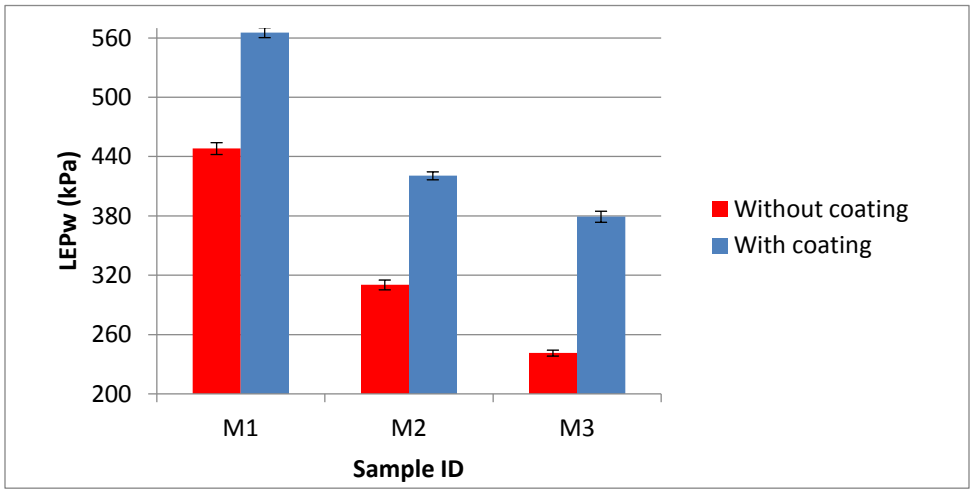

Figure 4-6. Effects of water content and nano-fibre coating

The average water contact angle (CAw) of the prepared membranes is represented in Fig. 4-7. The results show that, CAw decreased from 94° of M1 to 79° of M3 as the water content of the dope solution increased. It is evident that the increase in water content increases the hydrophilicity of the surface. Coating the surface of all the samples M1 to M3 with the nano-fibre layer increased CAw considerably, i.e. a 48% increase from M1 to M1C and 76% increase from M3 to M3C. As a result the highest CAw of 139° was achieved. This is ascribed to remarkable increase in the roughness parameter. For example, the average roughness parameter Ra for M1 before coating was 27.8 nm and 50.5 nm after coating (Fig. 4-8).

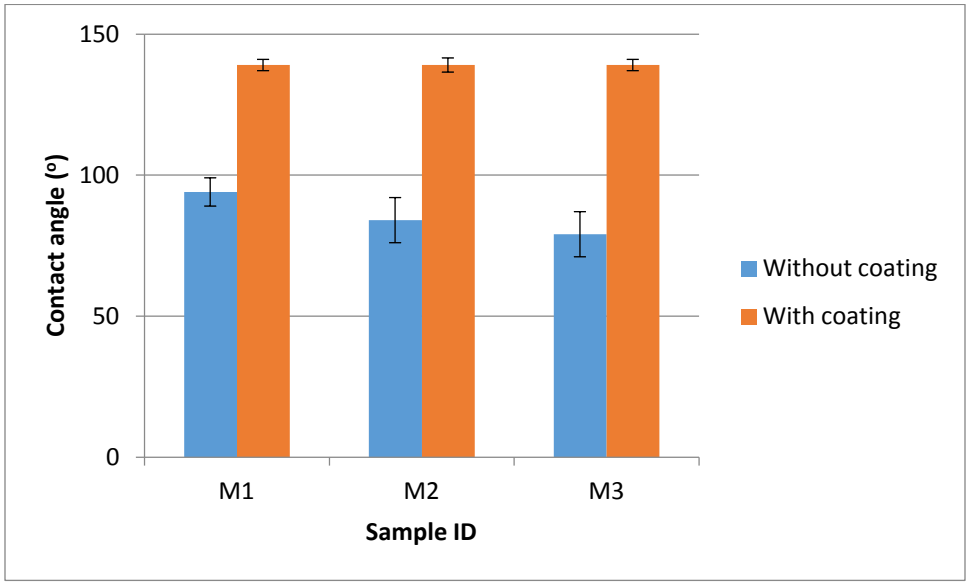

Figure 4-7. Contact angle analysis of coated and uncoated PVDF membranes

4.4.2 Performance analysis

4.4.2.1 VMD

All the prepared membranes were tested for VMD, both uncoated and coated with their performance data shown on Fig. 4-9. The feed solution was kept at 27^{o}C with an operating vacuum of 94.8kPa. The uncoated membranes were first tested before the coated membranes. From the results obtained, it could be seen that changing the water content from M1 to M3 did not have any significant effect on the VMD flux. By doubling the water content from M1 to M3, the flux could only be enhanced from 3.0 kg/m^2.h to 3.2 kg/m^2.h, a 6.6% increase. This further supports the fact that, though the pore sizes were enlarged by increasing the water content, the sponge-like layer which plays a key role in flux resistance was increased, as such there was a counter acting behaviour between pore size growth and flux resistance. Due to this, the enlarged pores could not deliver the high flux expected because the sponge-like layer resistance to mass transfer also increased [24] (Fig. 4-5).

Porosity analysis also revealed that, M1 had the highest porosity of 54% and M3 showed 46% porosity. This drop in porosity also ties with Fig. 4-5 as the sponge like layer becomes denser from M1 to M3.

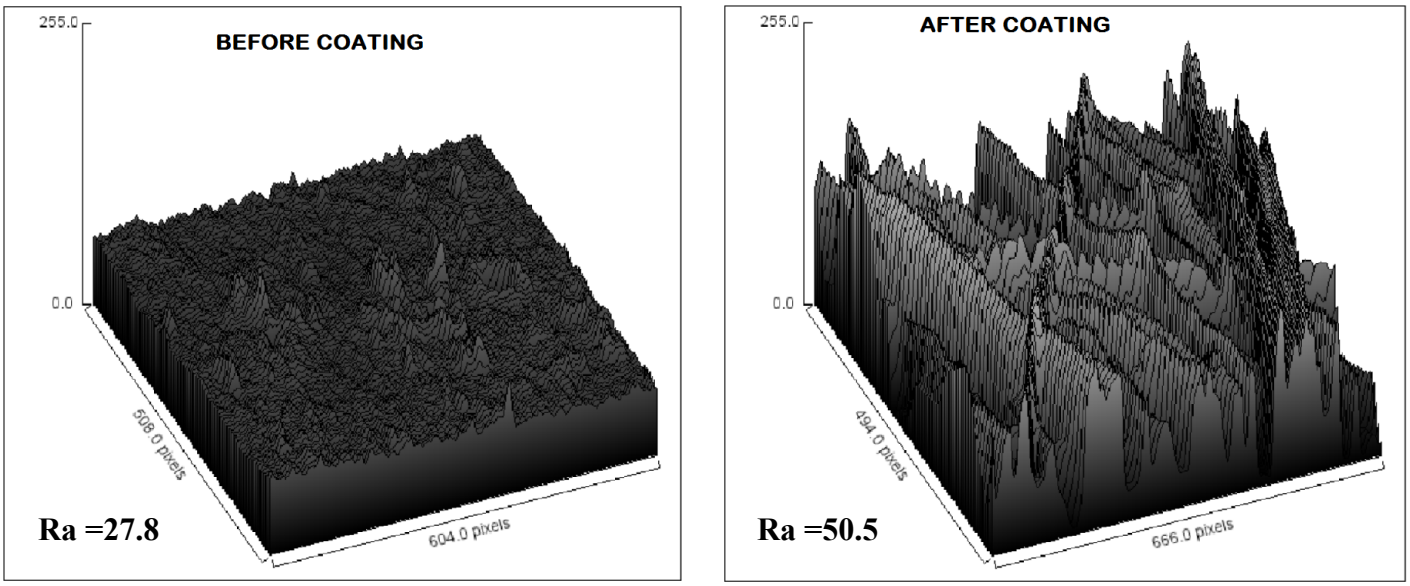

Figure 4-8. Roughness analysis images of M1 before and after coating.

Upon coating the substrate surface with a thin layer of nano-fibres, all the samples showed closely related results as the uncoated samples. This implies the extra layer of nano-fibres did not pose any significant resistance to mass transfer hence very minute decrease on the trans-membrane flux was experienced.

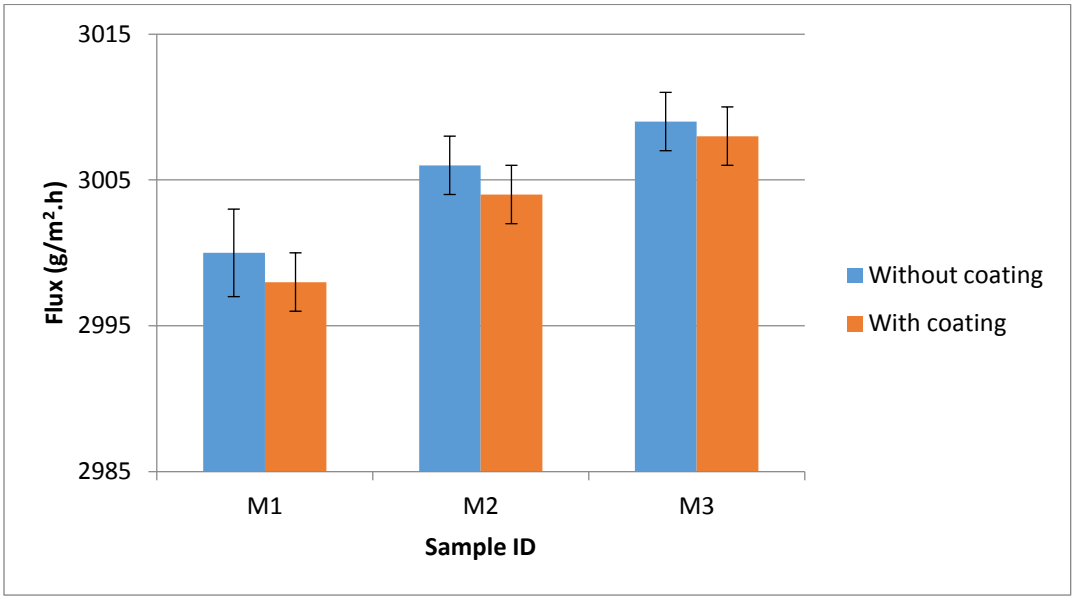

Figure 4-9. VMD flux results

It is of great importance to sustain the permeate flux and solute rejection during a practical MD application. A 6 h desalination process with 35 g/L NaCl feed solution was carried out. The results of the desalination process are summarized in Fig. 4-10. The conductivity of the distillate was less than 20 μS/m which indicated a salt rejection >99.98% for all the nano-fibres coated membranes. The permeate flux suffered a < 0.1% reduction from 3.0 to 2.9 kg/m^2.h for the first 2 h of the uncoated membrane (M3) and later gained it. But the nano-fibres coated membranes turn to produce a more stable flux all through the desalination process. This result show that for all the membranes fabricated, satisfying performance stability was achieved.

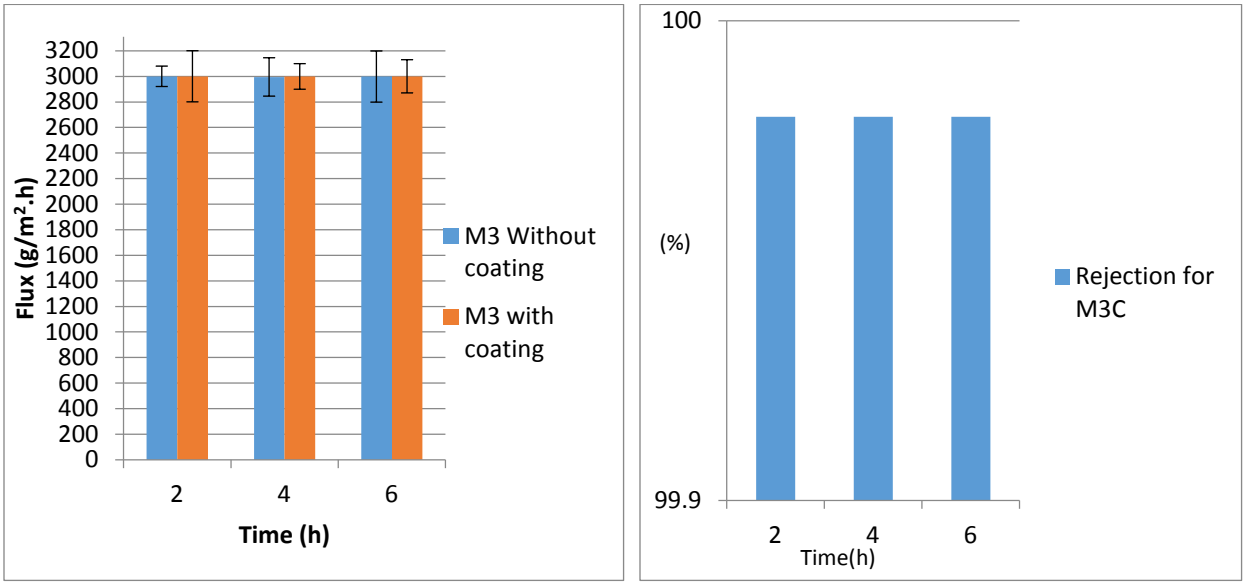

Figure 4-10. Flux and rejection analysis with time.

4.4.2.2 DCMD

The membrane M3C was also tested for using the DCMD setup in Fig. 4-2. The result of the DCMD flux obtained is shown on Fig. 4-11. The DCMD flux increases for sample M3C in DCMD. Since the coated membranes all have practically the same hydrophobicity, the change in flux is due to the change in water content in the casting dope that is responsible for the substrate pore enlargement. Also since the DCMD is a flow system, the mass transfer is greater than in the VMD static system and lesser effects of temperature polarization are seen which increases the driving force. Since surface and cross-section analyses showed an increase in finger-like macro-void layer across M1-M3 (uncoated), increasing the hydrophobicity turns to increase LEP_w, reduce pore wetting tendencies hence an increase in permeate flux. At lower temperatures DCMD has shown higher distillation flux than VMD because temperature losses due to conduction is minimal[21] and similar results of higher DCMD flux compared to VMD were reported by Koo et al [22]. Also since the dual layer membrane (Fig. 4-12) thickness ranges from

45-63 μm which is close to the range reported for dual layer membrane[23, 24], it implies heat losses in the DCMD will be minimal. The salt rejection obtained was >99.98%.

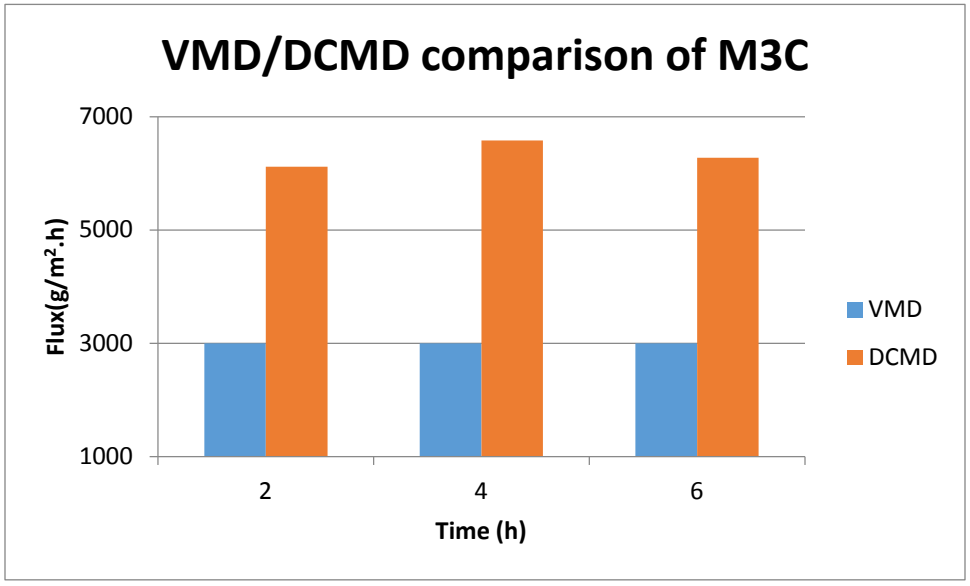

Figure 4-11. VMD/DCMD flux analysis of M3C membrane

To test the long term flux and rejection stability, DCMD experiments were carried out for 6 h with a 35 g/L NaCl feed solution at 27.5 ^{o}C while the cold side temperature was kept at 15±2^{o}C. The results were the same as those of the VMD, showing a stable flux with as little as 2% variations for the coated samples. This further confirms that, the nano-fibre coating helped prevent pore wetting over a prolonged period.

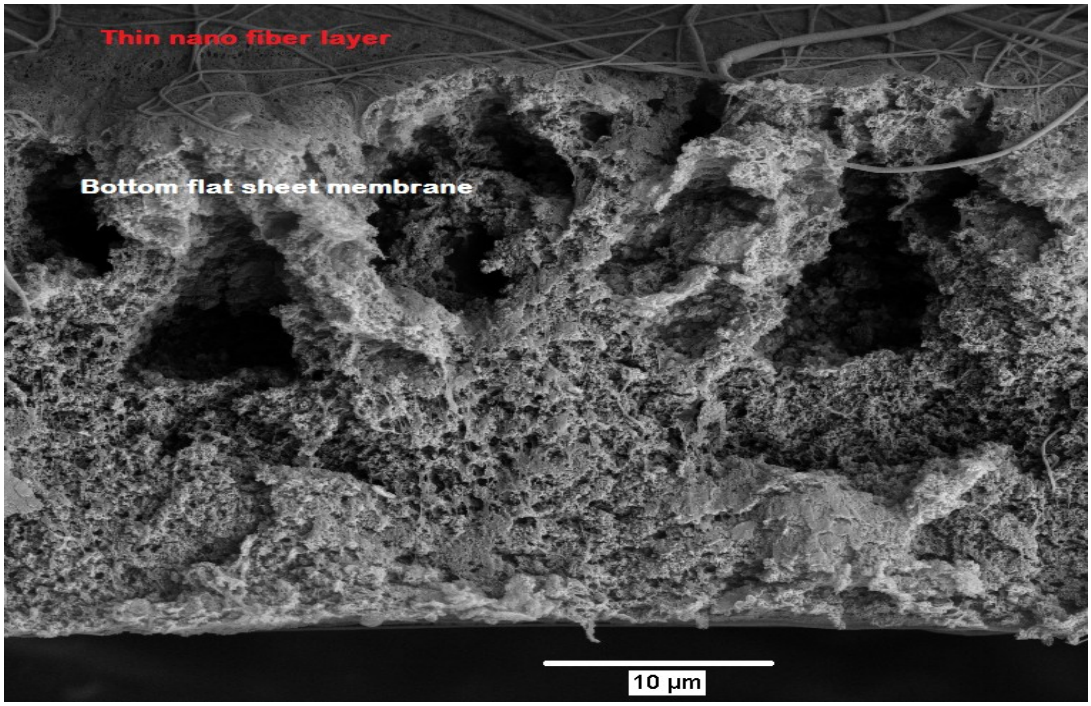

Figure 4-12. SEM image of the Dual layer membrane.

4.5 Conclusion

In this paper, a double layer membrane comprising of a bottom micro-porous PVDF nano composite flat sheet membrane, prepared by traditional phase inversion method and a top electro-spun nano-fibre thin layer was prepared and experimentally tested for desalination of synthetic NaCl salt solution by VMD and DCMD. The micro-porous PVDF membrane of the best performance obtained from our previous work contained 7 wt. % superhydrophobic SiO_2. In order to further improve the flux, the non-solvent (water) concentration in the dope solution was increased and also membrane surface coating with nano-fibre was made by electro-spinning. The flat sheet micro-porous membrane and the double layer membrane so prepared were characterized extensively. Increasing the water content of the dope solution reduced the water contact angle and LEP_w. Upon electro-spinning a thin layer of PVDF nano-fibres on the flat

sheet surface, the contact angle increased by 80%, which resulted in a 60% increase in LEP_w. The VMD flux of the double layer membrane was found to be similar to that of the flat sheet membrane while the salt rejection remained >99.98% for a 6 h operation. The DCMD flux of the double layer membrane was found to be doubled as high as VMD flux with a salt rejection greater than 99.98% when the experiment was carried out at the same feed temperature. Based on the results obtained, it can be concluded that electro-spinning a thin layer of nano-fibres on the surface has a favourable effect by increasing the contact angle and LEP_w and thus reducing pore wetting, which further enhances the membrane's long term stability. It can also be concluded that the double layer membrane developed in this work has a high prospect especially with respect to desalination by DCMD.

4.6 Acknowledgement

Special thanks to Arkema Inc. (Philadelphia, PA) for their generously offer of the polymers (Kynar® 740 and Kynar® HSV 900). Financial supports of the NSERC Discovery (Grant # RGPIN 288226-2010) and the I2IPJ (Grant # 463142-2014) grants are also gratefully acknowledged.

4.7 References

[1] Naidu, G., Jeong, S., Choi, Y., Jang, E., Hwang, T., & Vigneswaran, S. (2014). Application of vacuum membrane distillation for small scale drinking water production. *Desalination, 354*(0), 53–61.

[2] Drioli, E., Ali, A., & Macedonio, F. (2015). Membrane distillation: Recent developments and perspectives. *Desalination, 356*, 56–84.

[3] Kuo, C., Lin, H., Tsai, H., Wang, D., & Lai, J. (2008). Fabrication of a high hydrophobic PVDF membrane via nonsolvent induced phase separation. *Desalination, 233*(1-3), 40–47.

[4] Wang, P., & Chung, T. (2015). Recent advances in membrane distillation processes: Membrane development, configuration design and application exploring. *Journal of Membrane Science, 474*, 39–56.

[5] Tomaszewska, M., Gryta M., & Morawski, A. W. (2000). Mass transfer of HCl and H_2O across the hydrophobic membrane during membrane distillation, *Journal of Membrane Science, 166*, 149–157.

[6] Qtaishat, M., Khayet, M., & Matsuura, T. (2009). Novel porous composite hydrophobic/hydrophilic polysulfone membranes for desalination by direct contact membrane distillation. *Journal of Membrane Science, 341*(1–2), 139-148.

[7] Shirazi, M. M. A., Kargari, A., Tabatabaei, M., Ismail, A. F., & Matsuura, T. (2015). Assessment of atomic force microscopy for characterization of PTFE membranes for membrane distillation (MD) process. *Desalination and Water Treatment, 54*(2), 295-304.

[8] Fontananova, E., Jansen, J. C., Cristiano, A., Curcio, E., & Drioli, E. (2006). Effect of additives in the casting solution on the formation of PVDF membranes. *Desalination, 192*(1–3), 190–197.

[9] Bottino, A., Capannelli, G., A. Comite. (2002). Preparation and characterization of novel porous PVDF-ZrO_2 composite membrane, *Desalination*, *146*(0), 35–40.

[10] Liang, Y., Li, J.S., Sun, L., L.Wang, (2004). Study of the micro-structure of the nano- γ-Al_2O_3/PVDF hollow fibre membranes, *Technol. Water Treat. 30* (4), 199–201.

[11] Bae, T.H., Tak, T.M., (2005). Effects of TiO_2 nanoparticles on fouling mitigation of ultra-filtration membranes for activated sludge filtration, *Journal of Membrane Science, 249*, 1–8.

[12] Yang, Y., Rana, D., Matsuura, T., Zheng, S., & Lan, C. Q. (2014). Criteria for the selection of a support material to fabricate coated membranes for a life support device. *RSC Advances*, *4*(73), 38711–38717.

[13] Tijing, L. D., Choi, J., Lee, S., Kim, S., & Shon, H. K. (2014). Recent progress of membrane distillation using electrospun nanofibrous membrane. *Journal of Membrane Science, 453*(0), 435–462.

[14] Prince, J. A., Singh, G., Rana, D., Matsuura, T., Anbharasi, V., & Shanmugasundaram, T. S. (2012). Preparation and characterization of highly hydrophobic poly(vinylidene fluoride) – clay nanocomposite nanofibre membranes (PVDF–clay NNMs) for desalination using direct contact membrane distillation. *Journal of Membrane Science, 397–398*(0), 80–86.

[15] Prince, J. A., Rana, D., Singh, G., Matsuura, T., Jun Kai, T., & Shanmugasundaram, T. S. (2014). Nanofibre based triple layer hydro-philic/phobic membrane-a solution for pore wetting in membrane distillation. *Scientific Reports, 4(0),* 6949 (6 pp).

[16] Baghbanzadeh, M., Rana, D., Matsuura, T., & Lan, C. Q. (2015). Effects of hydrophilic CuO nanoparticles on properties and performance of PVDF VMD membranes. *Desalination*, *369*, 75–84.

[17] Chen, Z., Rana, D., Matsuura, T., Meng, D., & Lan, C. Q. (2015). Study on the structure and vacuum membrane distillation performance of PVDF membranes: I. Influence of molecular weight. *Chemical Engineering Journal, 276*, 174–184.

[18] Chen, Z., Rana, D., Matsuura, T., Yang, Y., & Lan, C. Q. (2014). Study on the structure and vacuum membrane distillation performance of PVDF composite membranes: I. Influence of blending. *Separation and Purification Technology, 133*, 303–312.

[19] Francis, L., Ghaffour, N., Alsaadi, A. S., Nunes, S. P., & Amy, G. L. (2014). PVDF hollow fibre and nanofibre membranes for fresh water reclamation using membrane distillation. *Journal of Materials Science, 49*(5), 2045–2053.

[20] Silva, T. L. S., Morales-Torres, S., Figueiredo, J. L., & Silva, A. M. T. (2015). Multi-walled carbon nanotube/PVDF blended membranes with sponge- and finger-like pores for direct contact membrane distillation. *Desalination, 357*(0), 233–245.

[21] Koo, J., Han, J., Sohn, J., Lee, S., & Hwang, T. (2013). Experimental comparison of direct contact membrane distillation (DCMD) with vacuum membrane distillation (VMD). *Desalination and Water Treatment, 51*(31-33), 6299–6309.

[22] Zhao, Y.-H. *et al.* (2008). Modification of porous poly(vinylidene fluoride) membrane using amphiphilic polymers with different structures in phase inversion process. *Journal of Membrane Science, 310*, 567–576.

[23] Bonyadi, S. & Chung, T. S. (2007).Flux enhancement in membrane distillation by fabrication ofdual layer hydrophilic–hydrophobic hollow fibre membranes. *Journal of Membrane Science, 306*, 134–146.

[24] Efome, J.E., et al (2015). Effects of superhydrophobic SiO_2 nanoparticles on the performance of PVDF flat sheets membranes for VMD, *desalination.* Doi.10.1016/j.desal.2015.07.002